Electronic Supplementary Information

for

Redox-inactive metal single-site molecular complexes: A new generation of electrocatalysts for oxygen evolution?

Tímea Benkó,[1] Dávid Lukács,[1] Krisztina Frey,[1] Miklós Németh,[1] Márta M. Móricz,[1] Dongyu Liu,[2] Éva Kováts,[3] Nóra V. May,[4] Lionel Vayssieres,[2] Mingtao Li,[2,*] József S. Pap[1,*]

[1]Centre for Energy Research, Institute for Energy Security and Environmental Safety, Surface Chemistry and Catalysis Department, 1121 Budapest, Konkoly-Thege street 29-33, Hungary

[2]International Research Center for Renewable Energy (IRCRE), State Key Laboratory of Multiphase Flow in Power Engineering (MFPE), Xi'an Jiaotong University, Xi'an 710049, China

[3]Institute for Solid State Physics and Optics, Wigner Research Centre for Physics, H-1525 Budapest, P.O. Box 49, Hungary

[4]Centre for Structural Science, Research Centre for Natural Sciences, Magyar tudósok körútja 2, Budapest, H-1117, Hungary

Contents

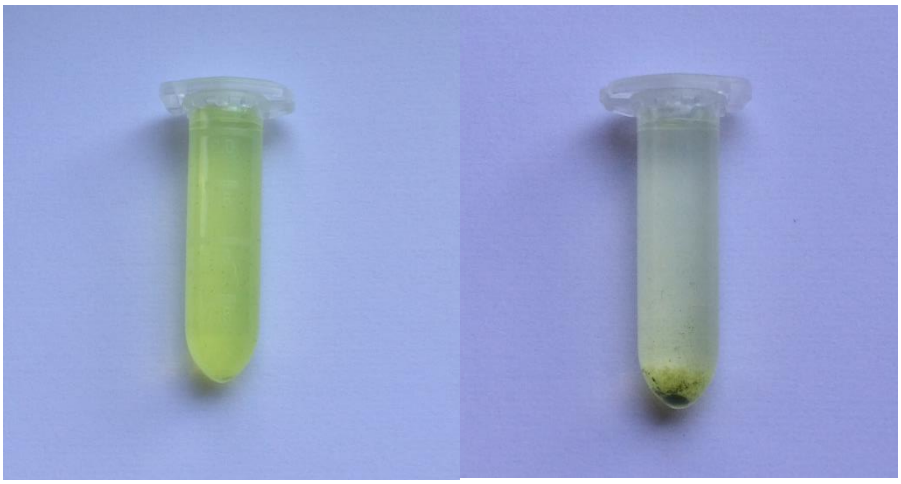

Figure S1. Solubility of **1** in pure water (on the left) and in 0.2 M carbonate buffer at pH 10 (on the right).

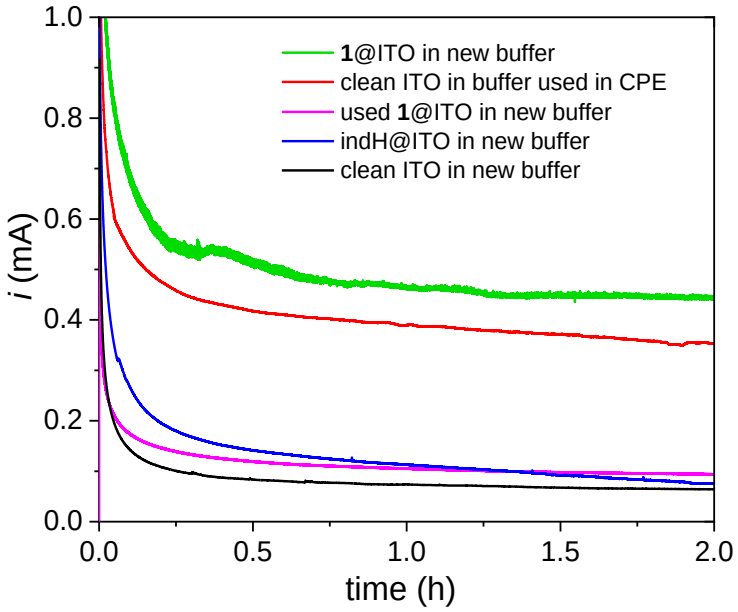

Figure S2. Comparison of controlled potential electrolysis current using **1**@ITO (0.6 μmol over 3 cm^2) at +1.4 V vs. Ag/AgCl ref in 0.2 M carbonate buffer at pH 10 (green), clean ITO in the same buffer after the first CPE (red), the used **1**@ITO in a new electrolyte (magenta), indH@ITO (0.6 μmol over 3 cm^2) in a new electrolyte (blue), and clean ITO in a new buffer.

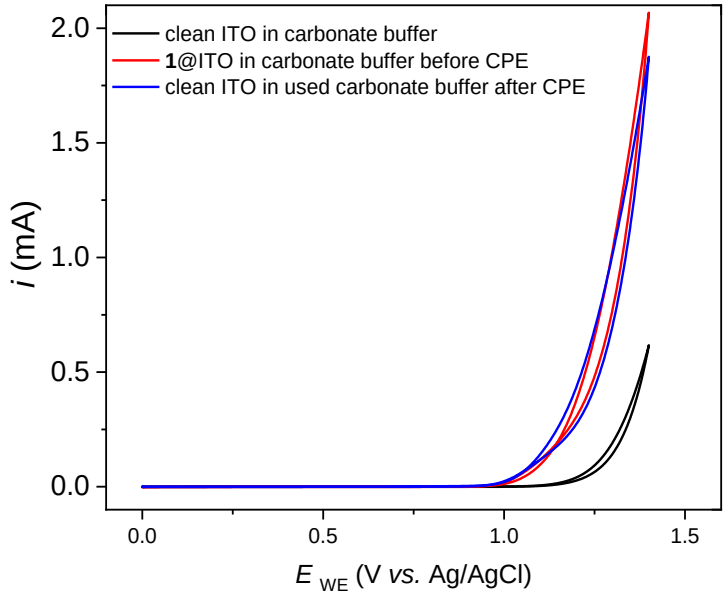

Figure S3. CV scans using **1**@ITO (0.6 μmol over 3 cm^2) at 100 mVs^{-1} in 0.2 M carbonate buffer at pH 10 (red), clean ITO in the same buffer after the CPE in Figure S2 (blue), and clean ITO in carbonate buffer at pH 10 (black). Note that the slight crossing of the CV branches near 1.1 V is due to a complex behavior that can be expected because of the dissolution, pre-catalyst transformation and possible partial re-adsorption of the catalyst on either the **1**@ITO modified electrode, or ITO immersed in the complex-saturated solution after CPE.

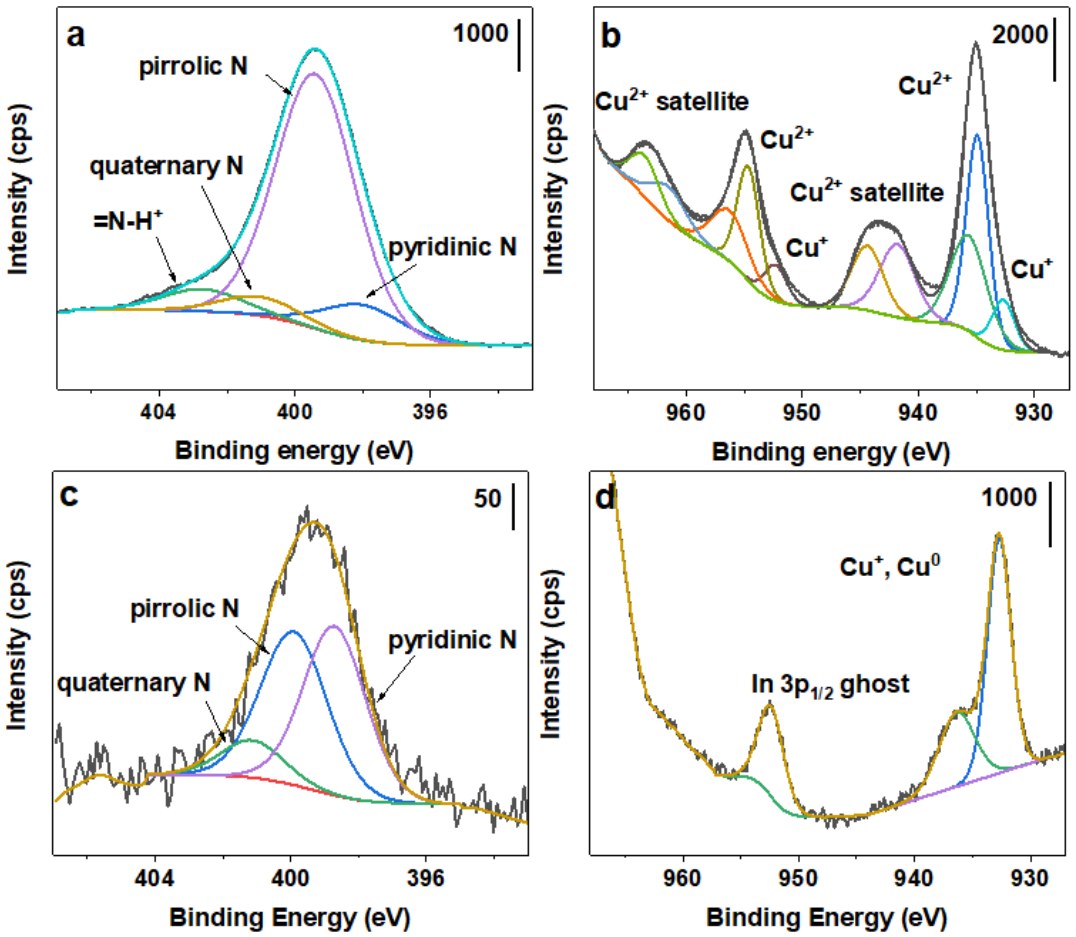

Figure S4. (a) The N 1s and (b) the Cu 2p binding energy region of XP spectra of the as-prepared **1**@ITO (black line) with the fitted components in colours; (c) and (d) the corresponding spectra after 20 hours of CPE (see Fig. 2a in the main text).

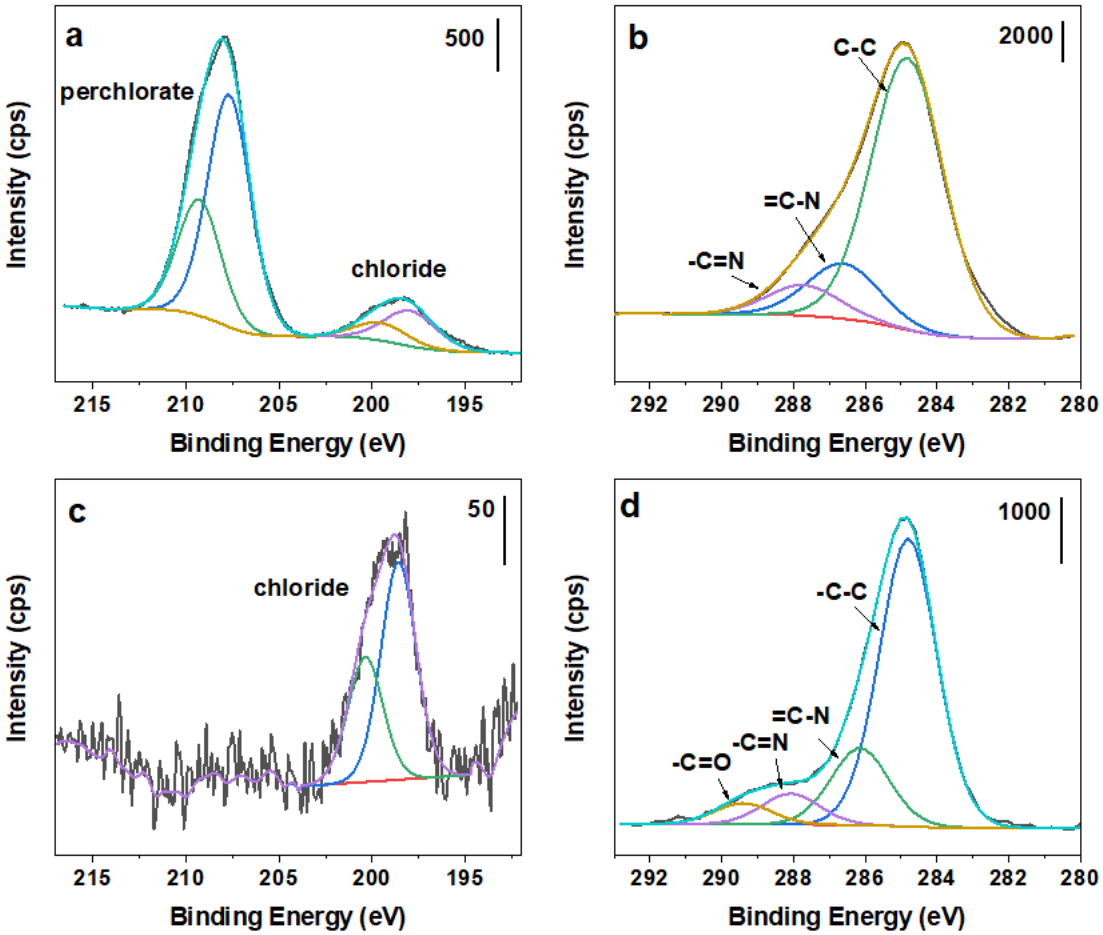

Figure S5. (a) The Cl 2p and (b) the C 1s core level XP spectrum of the as-prepared **1**@ITO (black line) with the fitted components in colours; (c) and (d) the corresponding spectra after 20 hours of CPE (see Fig. 2a in the main text).

Table S1. Selected binding energy values from the fitting of XP spectra of the as prepared **1**@ITO, and of those collected after 20 h of CPE at +1.4 V vs. Ag/AgCl in carbonate buffer at pH 10 (in parenthesis).

Elements / Component Peak	Binding Energy (eV) as prepared	Chemical State after 20 h
N 1s 1	398.2 (398.7)	pyridinic N
N 1s 2	399.5 (399.9)	pirrolic N
N 1s 3	401.2 (401.2)	quaternary N
N 1s 4	402.7	$=N\text{-}H^{+}$
Cu 2p 1	932.7 (932.7)	Cu^{+}
Cu 2p 2	934.9	Cu^{2+}
Cu 2p 3	935.8	Cu^{2+}
Cu 2p 4	941.8	satellite
Cu 2p 5	944.4	satellite
Cu 2p 6	952.4(952.5)	Cu^{+}
Cu 2p 7	954.7	Cu^{2+}
Cu 2p 8	956.6	Cu^{2+}
Cu 2p 9	961.7	satellite
Cu 2p 10	963.9	satellite
Cl 2p 1	207.7	ClO_4^{-}
Cl 2p 2	209.3	ClO_4^{-}
Cl 2p 3	198.1 (198.6)	Cl^{-}
Cl 2p 4	199.8 (200.3)	Cl^{-}

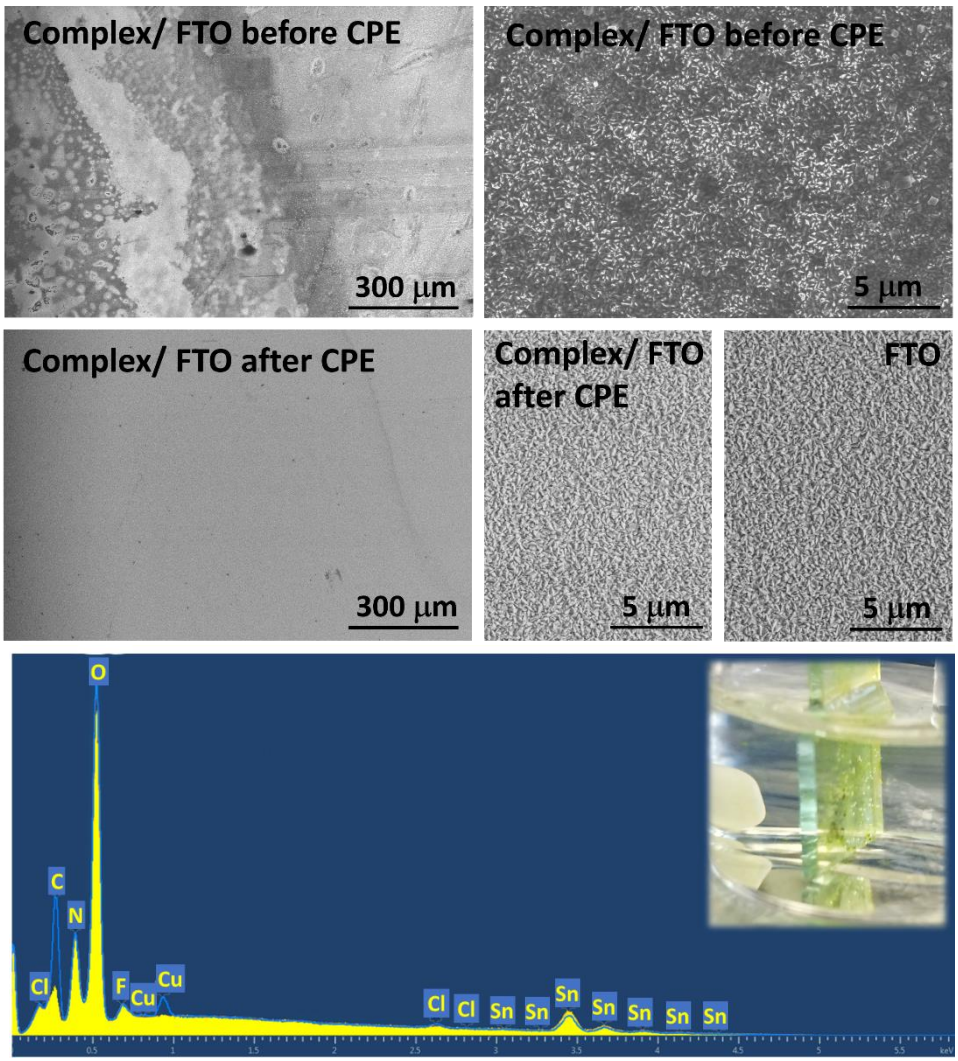

Figure S6. SEM image of an as-prepared **1**@FTO (0.2 μmol over 3 cm^2) sample and following CPE at +1.2 V vs. Ag/AgCl ref in 0.2 M carbonate buffer at pH 10 for 20 minutes. Experimentals for SEM: 5 kV beam accelerating voltage, 0.10 nA probe current, Everhart-Thornley detector, operation for secondary electron, 6.9 mm working distance. The detection mode was optimized for horizontal plane with short working distance. Bottom: the EDX spectrum of the **1**@FTO electrode before (yellow) and after CPE (light blue line). Inset: picture of the electrode taken in the course of CPE.

Electrolysis experiments with 1@FTO electrode

We conducted CPE experiments by using fluorine doped tin-oxide (FTO) with higher surface roughness (600 nm) instead of the ITO support, in order to investigate the effect of the support on the stability of the complex layer. In this case the current was lower than in the case of ITO, due to poorer surface coverage and the lower potential (+1.2 V vs. Ag/AgCl) applied for CPE. The surface morphology of the sample was analysed by scanning electron microscopy (SEM), and its composition by energy dispersive X-ray spectroscopy (EDX). The SEM images of **1**@FTO before CPE (Fig. S6) show well distributed crystallites on the surface, whereas after the CPE experiment a quasi-clear surface can be observed. The SEM picture at x5000 magnification shows the surface of a clean FTO electrode, where dark patches signal

the presence of the complex on with the **1**@FTO. The elemental composition by EDX is consistent with the expected presence of C, N, O, Cu and Cl for **1**, or a derivative still containing perchlorate. After only 20 minutes of CPE Cu and C completely disappear and the same homogeneous process takes place like in the case of ITO.

Table S2. Crystal structure details for **2**·CH_3OH and **3**.

	2·CH_3OH	**3**
Chemical formula	$C_{19}H_{18}ClCuN_5O_6$	$C_{28}H_{20.5}Cl_{0.5}Cu_{1.5}N_{7.5}O_4$
Formula weight	511.37	639.05
Radiation type	Mo Kα	Cu Kα
Space group	triclinic, P–1	triclinic, P–1
a (Å)	7.8810(2)	12.4454(3)
b (Å)	10.7847(3)	13.2667(4)
c (Å)	12.0770(4)	16.8433(5)
α (°)	91.738(2)	76.118(2)
β (°)	105.882(2)	87.983(2)
γ (°)	95.876(2)	82.560(2)
V (Å^3)	980.28(5)	2677.01(13)
Z	2	4
D_{calc} (Mgm^{-3})	1.732	1.586
Crystal dimensions (mm)	0.1×0.1×0.05	0.2×0.2×0.08
Temperature (K)	100.0(1)	100.0(1)
Unique reflections	4791	10968
Θ_{min}	29.690	76.307
Θ_{max}	3.123	3.459
μ	1.302	2.446
Data > 2σ/parameters/restraints	3901/357/0	9276/750/0
R^a [$F^2 > 2\sigma(F^2)$], wR^b (F^2)	0.0390, 0.0835	0.0383, 0.0958
Goodness of fit (GOF)	1.059	1.020

[a] $R = \Sigma||F_o| - |F_c||/\Sigma|F_o|$.

[b] $wR = [\Sigma w(F_o^2 - F_c^2)^2/\Sigma w(F_o^2)^2]^{1/2}$, $w = 1/\sigma^2(F_o)^2 + (AP)^2 + BP$, where $P = [F_o^2 + 2F_c^2]/3$, A = 0.0359, 0.0516; B = 0.8485, 0.9383, for **2**·CH_3OH and **3**, respectively

Table S3. Selected bond distances (Å) and angles (°) for complex **3.**

Bond distances	(Å)
Cu01–O1	1.9804(14)
Cu01–N1	1.9045(17)
Cu01–N2	2.0110(19)
Cu01–N6	2.0066(19)
Cu02–O3	1.9599(16)
Cu02–N7	2.026(2)
Cu02–N8	1.889(2)
Cu02–N9	2.027(2)
Cu03–O2	1.9620(15)
Cu03–N4	2.028(2)
Cu03–N12	2.027(2)
Cu03–N13	1.906(2)

Bond angles	(°)
O1–Cu01–N2	90.68(7)
O1–Cu01–N6	90.25(7)
N1–Cu01–O1	154.17(7)
N1–Cu01–N2	90.95(8)
N1–Cu01–N6	90.75(8)
N6–Cu01–N2	174.11(8)
O3–Cu02–N7	91.61(8)
O3–Cu02–N9	90.27(8)
N7–Cu02–N9	165.40(8)
N8–Cu02–O3	165.63(7)
N8–Cu02–N7	91.38(9)
N8–Cu02–N9	90.37(9)
O2–Cu03–N4	90.01(7)
O2–Cu03–N12	92.83(8)
N12–Cu03–N4	169.93(8)
N13–Cu03–O2	157.71(8)
N13–Cu03–N4	89.71(9)
N13–Cu03–N12	91.32(10)

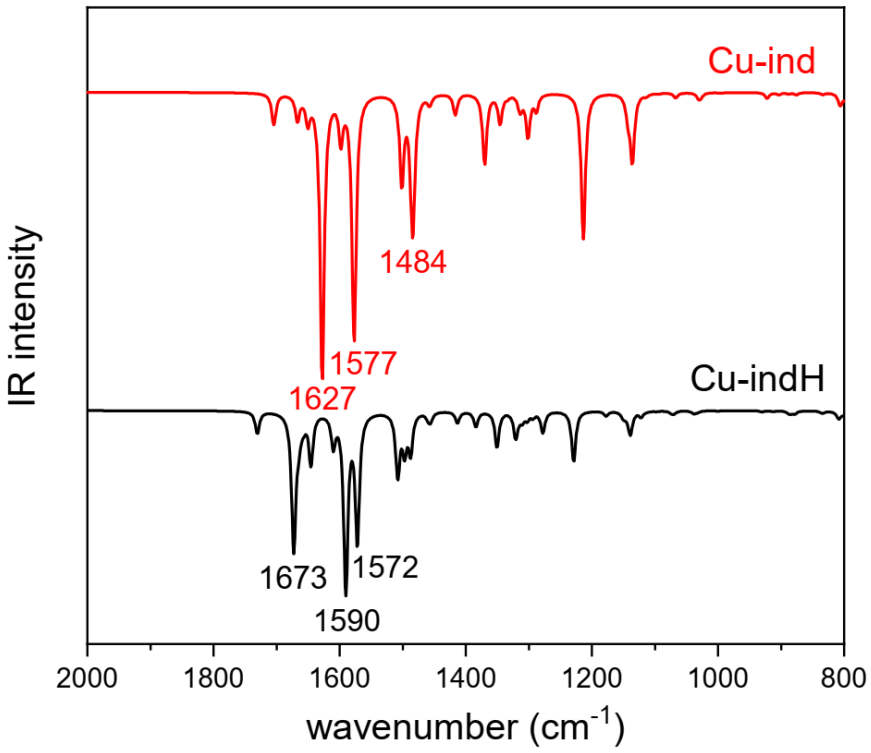

Figure S7. Computational IR spectra of $[Cu(ind)]^{+}$ and $[Cu(indH)]^{2+}$ in water.

We have constructed the IR spectra for the Cu-ind^{-} and Cu-indH moieties in water. The C=N mixed vibration absorption peaks around 1600 cm^{-1} are in qualitative agreement with the experimental results (Fig. 2b), where the proton on the ligand (i.e., indH) would extend the absorption edge of the large wavenumber side.

Computational studies of the fifth ligand in aqueous solution

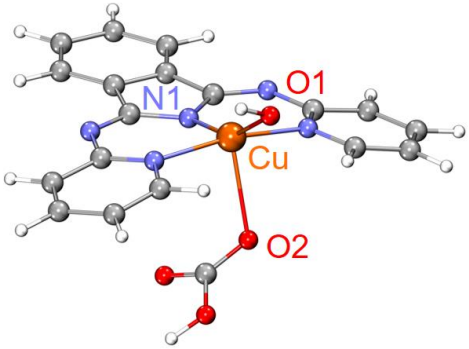

$[Cu^{II}(ind)(OH)(HCO_3)]^-$

d_{Cu-O1} = 1.95 Å $\angle_{N1-Cu-O1}$ = 152.42°
d_{Cu-O2} = 2.41 Å $\angle_{N1-Cu-O2}$ = 104.15°

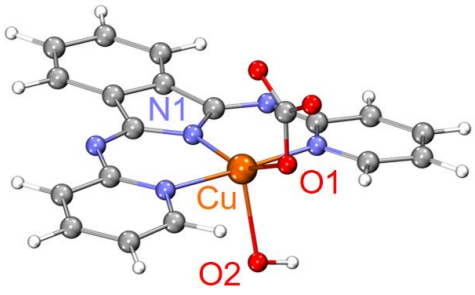

$[Cu^{II}(ind)(OH)(CO_3)]^{2-}$

d_{Cu-O1} = 2.01 Å $\angle_{N1-Cu-O1}$ = 152.88°
d_{Cu-O2} = 2.19 Å $\angle_{N1-Cu-O2}$ = 109.11°

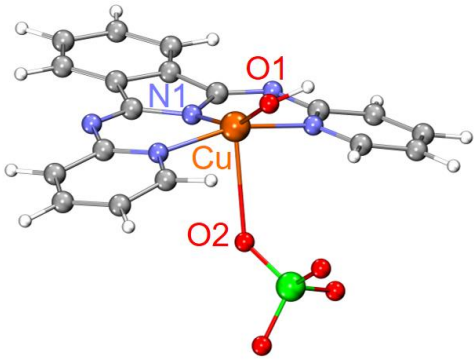

$[Cu^{II}(ind)(OH)(ClO_4)]^-$

d_{Cu-O1} = 1.93 Å $\angle_{N1-Cu-O1}$ = 155.62°
d_{Cu-O2} = 2.63 Å $\angle_{N1-Cu-O2}$ = 96.14°

Figure S8. Optimized structures of [Cu(ind)(OH)] with HCO_3^-, CO_3^{2-}, and ClO_4^- species as the additional ligand in aqueous solution.

Since the Cu(II) is more favorable to form a square planar configuration, the Cu-ind$^-$ complex could only accept one more ligand with strong interaction. Therefore, in aqueous solution at pH 10, HO^- need to compete with other solvent molecules to occupy the reaction site. For HCO_3^- and ClO_4^-, the longer Cu–O bond length indicates a weaker interaction, and these two species are unlikely to affect the reaction. While for CO_3^{2-}, the shorter Cu–O bond length represents that it has replaced HO^- on the strongly bonded reaction site. This configuration would greatly reduce the interplay between Cu^{II} and HO^-, thus quenching the catalysis. However, the CO_3^{2-} can act as the proton acceptor during the reaction and be protonated to form HCO_3^-, then it will leave the reaction site as discussed above and the water oxidation could restart. Colour code: grey for C, blue for N, orange for Cu, red for O, green for Cl, and white for H.

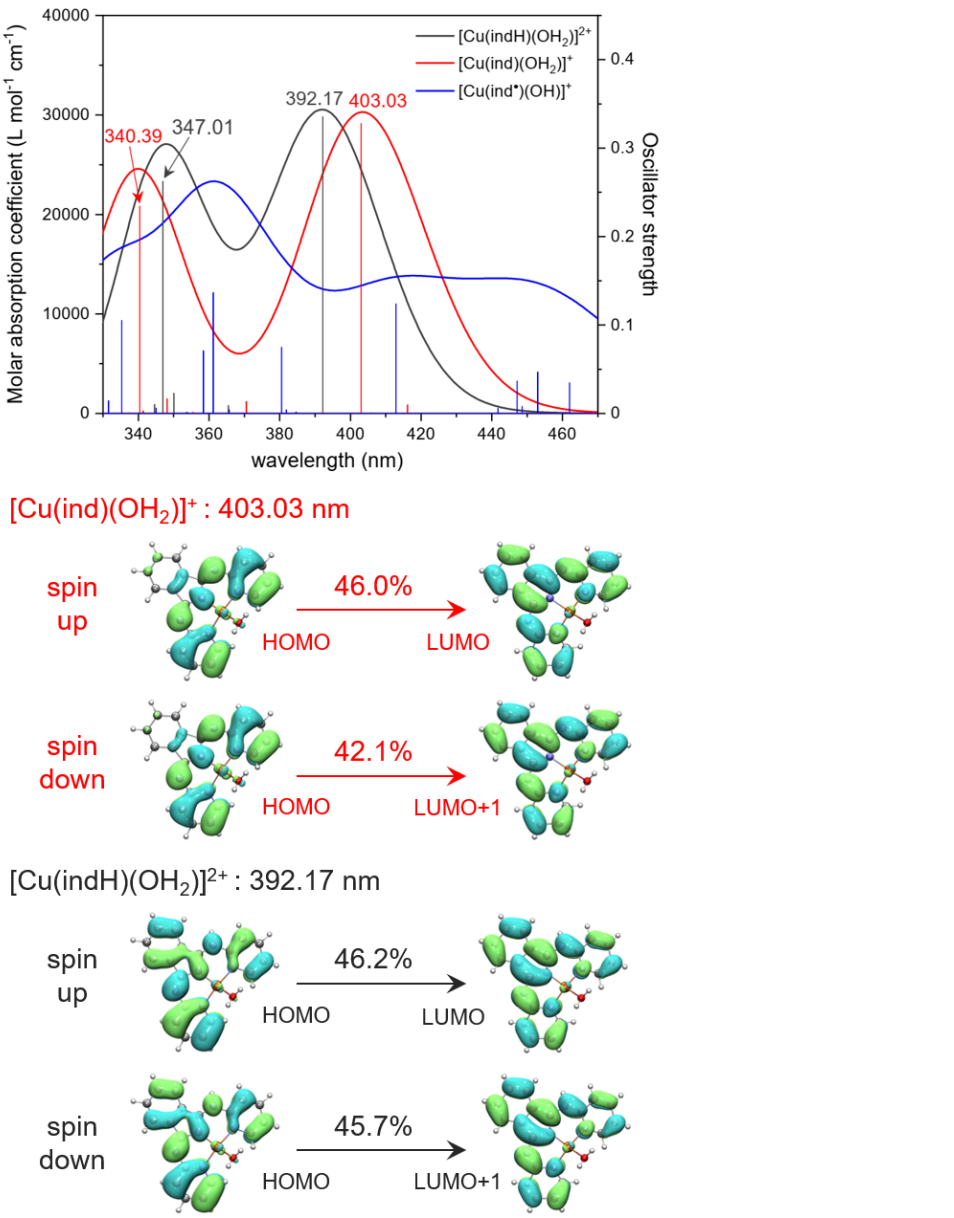

Figure S9a. Computational UV-vis spectra of Cu-indH, Cu-ind, and Cu-ind• in acetonitrile (top). The lines represent the oscillator strengths of the individual transitions. The molecular orbitals involved in the excitations with the wavelength around 400 nm and their contributions are also given. The additional proton in Cu-indH would affect the HOMO a lot and induce a negative absorption peak shift of about 10 nm, which is consistent with the experimental results. While the spectrum of Cu-ind• in acetonitrile is substantially different around this region. These results confirm that the UV-vis spectra change in Fig. 5b is corresponding to the protonation of the ligand instead of oxidation of the ligand.

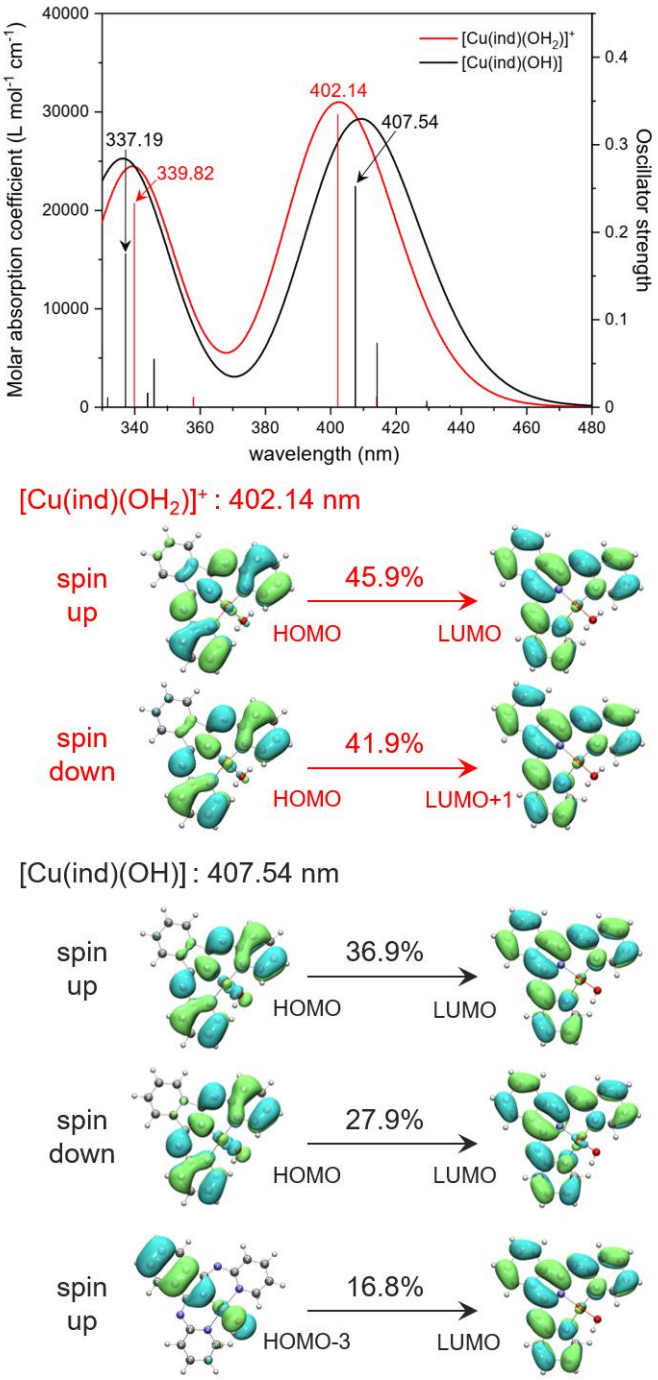

Figure S9b. Computational UV-vis spectra of Cu-ind with the additional OH_2 or OH ligand in water. The lines represent the oscillator strengths of the individual transitions. The molecular orbitals involved in the excitations with the wavelength around 400 nm and their contributions are also given. The deprotonation of H_2O will rarely the HOMO and LUMO of the complex, which are mainly comprised by the ind ligand. However, the HOMO-3 (spin up) is additionally introduced into this excitation. Computational results show that the deprotonation effect will rarely change the absorption wavelength (about 5 nm), but reduce the oscillator strength.

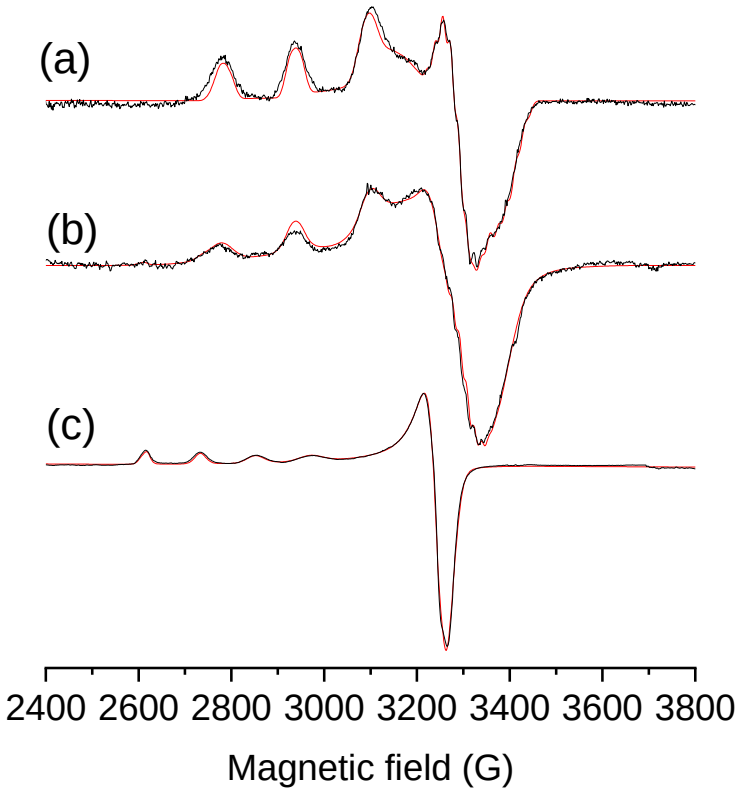

Figure S10. Experimental (black) and simulated (red) EPR spectra recorded at 77K for (a) **2** (0.4 mM) in ethanol/aqueous mixture, (b) **2** (0.2 mM) in ethylene-glycol/aqueous mixture, and (c) $Cu(ClO_4)_2$ (~1 mM) in ethylene-glycol/aqueous mixture.

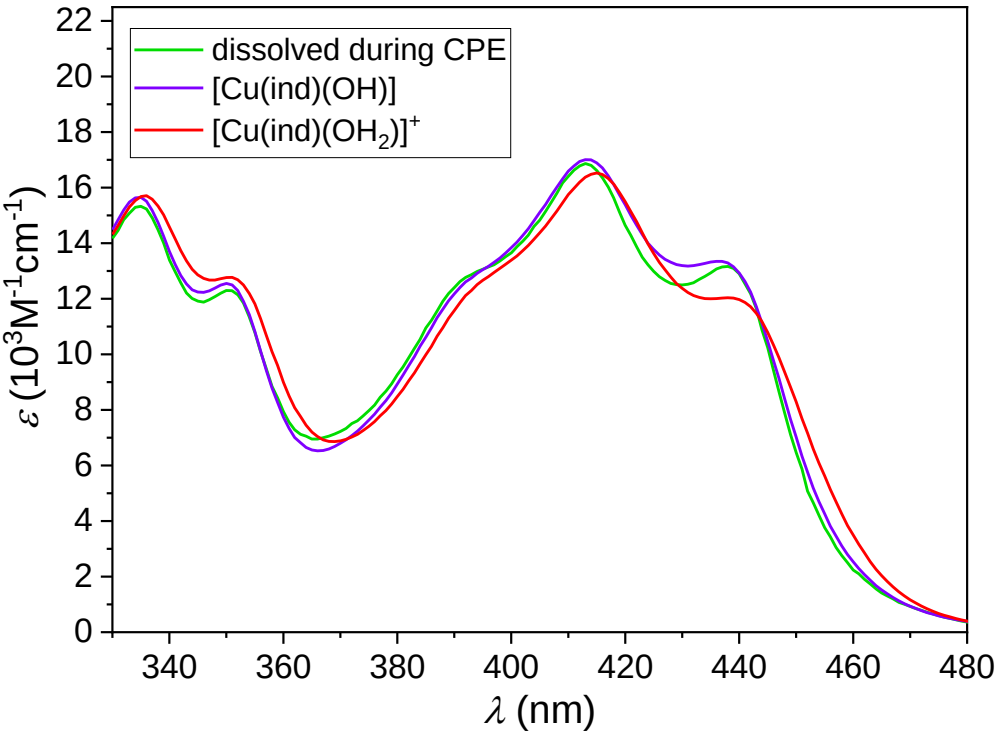

Figure S11. Experimental UV-vis absorption spectra for **2** at pH 9.3 (red), pH 10.9 (purple) and the spectrum measured in in the carbonate buffer after CPE using **1**@ITO.

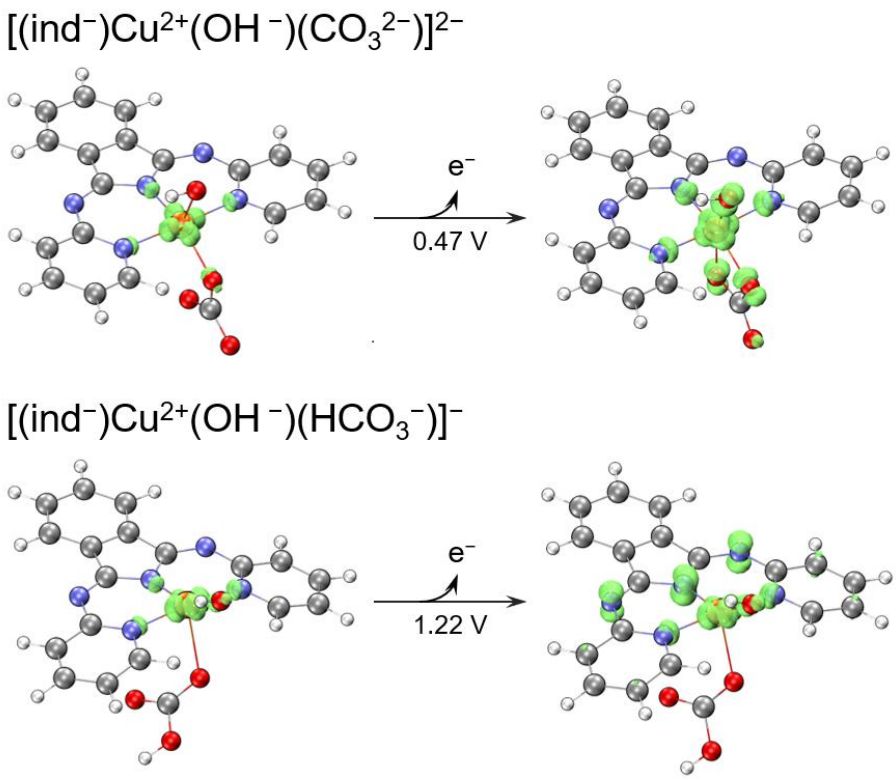

Figure S12. Spin density changes and the DFT calculated redox potentials (*vs*. NHE) of oxidizing the complex with the carbonate/bicarbonate ligand**.** The results show that CO_3^{2-} could participate in the oxidation reaction (electron loss) inducing a relatively low redox potential. However, this redox peak is not observed in the experiments. Given CO_3^{2-} is in equilibrium with HCO_3^- at pH 10, a similar oxidation was also investigated by DFT for a $[Cu(ind)(OH)(HCO_3)]^-$ form. According to our results, bicarbonate will not participate in the oxidation reaction anymore and the computational redox potential is comparable with the experimental value. Therefore, the carbonate buffer is unlikely to be oxidized during the reaction.

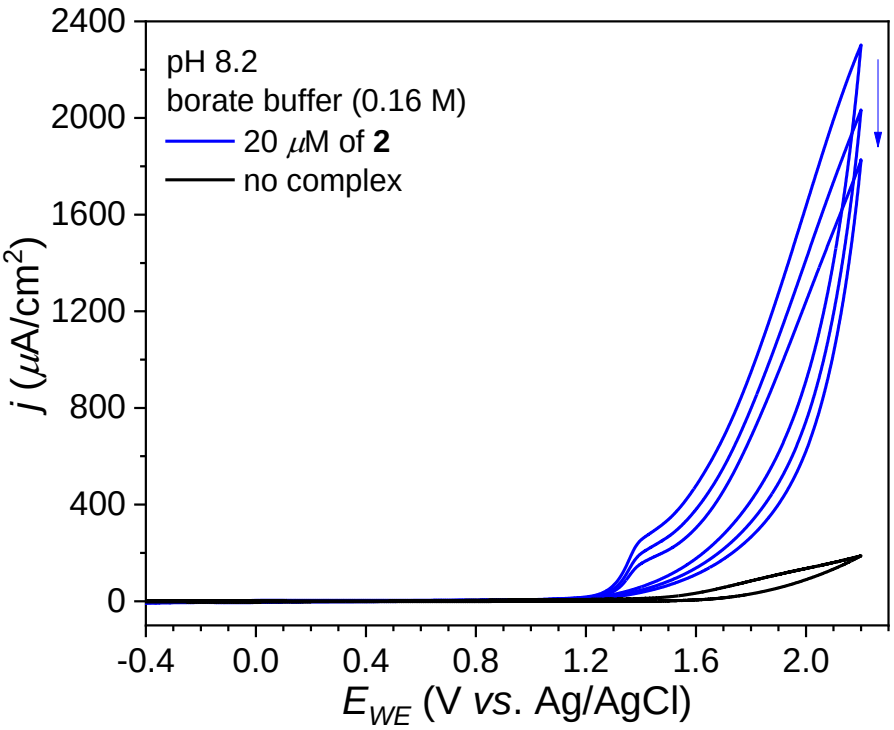

Figure S13. Cyclic voltamogram of **2** (20 μM) in borate buffer (0.16 M) at pH 8.2 (blue curve) and background current of the BDD working electrode in a pure buffer under the same conditions (under Ar, at 100 mV/s).

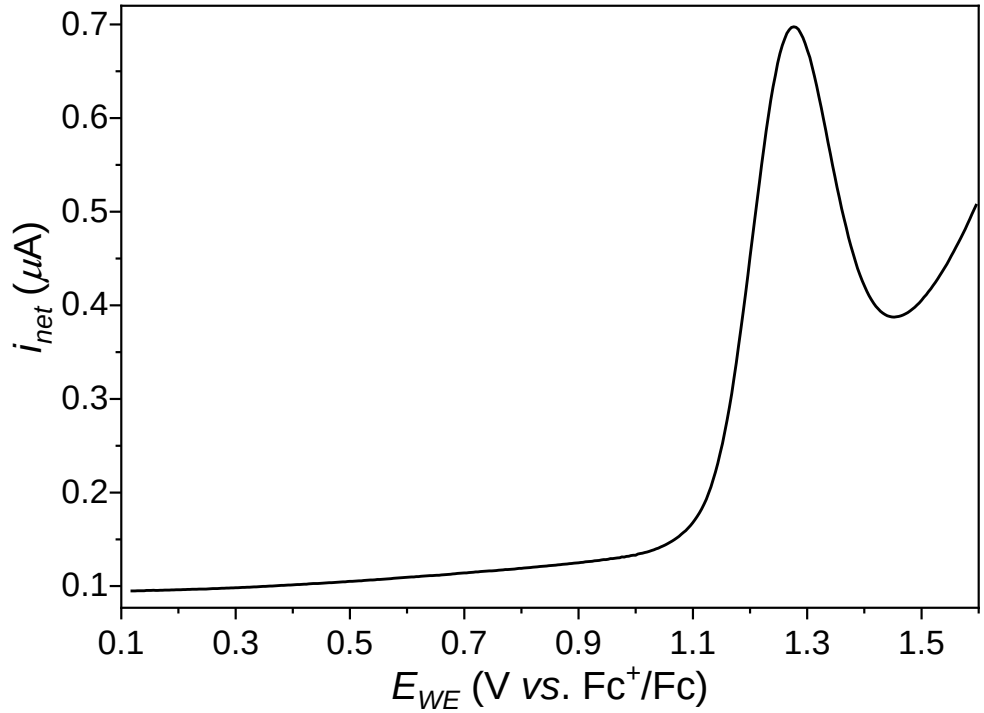

Figure S14. SWV for indH (0.05 mM) in acetonitrile, 0.1 M TBAP, BDD working electrode, under Ar, P_H = 32 mV; P_w = 80 ms; S_H = 4 mV**.**

Titration of 1 in acetonitrile in the absence of water

The addition of the complex to a 0.1 M TBAP solution increases the electrolytic conductivity and only one cathodic $Cu^{II/I}$ peak is present in SWV at -0.41 V *vs*. Fc^+/Fc (Fig. S15). These facts indicate a single cationic form for which the absorbance at 418 nm (see the spectrum of **1** in Fig. S16) and 717 nm increases linearly with the total complex concentration (Fig. S17). In contrast, when TBAP is absent the equilibria shift (Fig. S17) that is readily explained by the dissociation of the second, inner-sphere perchlorate.

Titration of the complex with *n*-butylamine in acetonitrile containing 0.1 M TBAP reproduces the UV-vis spectral changes (Fig. S16) observed earlier by titration with triethylamine, with which the pK_a of the complex according to eq. (1) was reported as 10.55 (see ref. 38 in the main text). This high value indicates the presence of Cu-indH in an aprotic solvent.

$$[Cu^{II}(indH)(NCCH_3)(OClO_3)]^+ + Et_3N = [Cu^{II}(ind)(NCCH_3)(OClO_3)] + Et_3NH^+ \quad (1)$$

The clear isosbestic points at 265, 295, 336 and 406 nm indicate that only two absorbing species are present and the increase at 418 nm and 444 nm shows the conversion to the deprotonated form of the complex.

SWV shows the oxidation peak at +1.31 V *vs*. Fc^+/Fc increasing with added *n*-butylamine (Fig. S15) suggesting in turn that the $[Cu^{II}(ind)(NCCH_3)(OClO_3)]^+$ form is involved in this oxidation containing the deprotonated ind^-. Simultaneously, the reduction peak at -0.41 V *vs*. Fc^+/Fc is decreased and another one at -0.84 V *vs*. Fc^+/Fc occurs instead. The ratio of the peak areas changes in the function of *n*-butylamine concentration indicating a transition between two different protonation states of the complex in agreement with the UV-vis titration. The peak at -0.41 V *vs*. Fc^+/Fc can be assigned to the $[Cu^{II}(indH)(NCCH_3)(OClO_3)]^+ + e^-$, while the peak at -0.84 V *vs*. Fc^+/Fc to the $[Cu^{II}(ind)(NCCH_3)(OClO_3)]^+ + e^-$ reduction.

To sum up, the complex participates in equilibrium between the protonated and deprotonated forms and the corresponding redox transitions in acetonitrile also dependent on the perchlorate excess (Fig. S18). The oxidation of the ligand can be associated with the deprotonated form, while Cu-indH is oxidized only at higher potentials.

The difference UV-vis spectra recorded upon bulk oxidation of **1** at +1.52 V *vs*. Fc^+/Fc on ITO (Fig. S19) reveal a growth in the two most characteristic bands of the deprotonated ligand at 418 nm and 444 nm. Thus, if the Cu-$ind^{\bullet}$ oxidation state is generated electrochemically, in a follow-up chemical reduction it produces Cu-ind^-, where the proton is missing from the ligand. Importantly, no sign of LMCT bands typical for d^8 Cu^{III} could be detected in the differential electronic spectra in accordance with DFT.

Behavior of 1 in acetonitrile in the presence of water

Addition of water to **1** in acetonitrile induces two events. The coordinated indH ligand loses a proton to bulk water setting an acid-base equilibrium and the coordinated acetonitrile exchanges with aqua ligand. The former equilibrium becomes obvious from the UV-vis spectroscopic features in water being similar to those of the titration of **1** with *n*-butylamine in acetonitrile. In the presence of 0.1 M TBAP one perchlorate remains in the coordination sphere, thus the acid-base equilibrium constant can be given as K =

$[Cu(ind)(OClO_3)(X)][H_3O^+]/\{[Cu(indH)(OClO_3)(X)^+][H_2O]\}$ = 8.5(4)×10^{-7} (X = solvent) in water-acetonitrile mixtures. Note that the indH/ind$^-$ equilibrium with added water allows to estimate the initial proportion of $[Cu^{II}(ind)(OClO_3)(X)]$. Addition of water causes a slight bathochromic shift in the Cu d-d transition also indicative of ligand exchange. When only H_2O is present (no excess perchlorate), it can act as ligand and proton acceptor to furnish predominantly the $[Cu^{II}(ind)(OH_2)]^+$ equilibrium form over $[Cu^{II}(indH)(NCCH_3)(OClO_3)]^+$ as ind$^-$ favors perchlorate dissociation leading to the form responsible for catalysis.

In the presence of H_2O the CVs show similar behavior to those of **2** (Fig. S20). In the presence of TBAP the increased current should originate from $[Cu^{II}(ind)(OH_2)(OClO_3)]$ accumulated by the dual effect of water. Peaks in SWV reveal a second oxidation at +1.48 V *vs*. Fc$^+$/Fc that is similar to that of **2** (Fig. 10a, see Fig. S21) overlapped with the first one, the area of which showing linear dependence on $[H_2O]$ (Fig. S21, inset), in agreement with the increase in the deprotonated form the same way as in the case of *n*-butylamine titration.

Estimation of acid-base dissociation constant of $[Cu^{II}(indH)(OClO_3)]^+$ in acetonitrile-water mixture

The determination based upon pH measurements and pH conversion.[1] The complex solubilized with 80 w/w% MeCN and 20 w/w% water mixture with acetonitrile molar ratio of 0.637. For the concentration dependent pH scale the density was calculated: ρ = 0.828 kg/l.

$pH_{corr} = pH_{measured} - \delta_c$, where $\delta_c = \delta_c^0 + \log_{10}(\rho)$.

After that tetrabutylammonium perchlorate salt was added to make 0.1 M TBAP containing mixture. The measurement was carried out the next day. The experimental data for higher complex concentrations is more reliable (lower standard error) because at small complex concentration the pH equilibrium can be reached later, and KCl from the probe reference solution or $KClO_4$ (from TBAP + KCl reaction) can precipitate – because of the low solubility in the mixture – at the pH probe membrane and terminates the measurement by breaking the circuit.

The inner-sphere perchlorate containing complex is the dominant form next to 0.1 M TBAP, which can be deprotonated by water.

$$K = \frac{[Cu(ind)(NCCH_3)(OClO_3)][H_3O^+]}{[Cu(indH)(NCCH_3)(OClO_3)^+][H_2O]}$$

In the 0.4 mM – 1 mM complex concentration range K = 8.5(4)×10^{-7} (~5% std. error). From this at 0.1 mM complex concentration with 2 M water present, the deprotonated form is roughly 12% of the total.

[1] Gagliardi, L. G.; Castells, C. B.; Ràfols, C.; Rosés, M.; Bosch, E. δ Conversion Parameter between pH Scales (and) in Acetonitrile/Water Mixtures at Various Compositions and Temperatures. *Anal. Chem.* **2007**, *79* (8), 3180–3187. https://doi.org/10.1021/ac062372h.

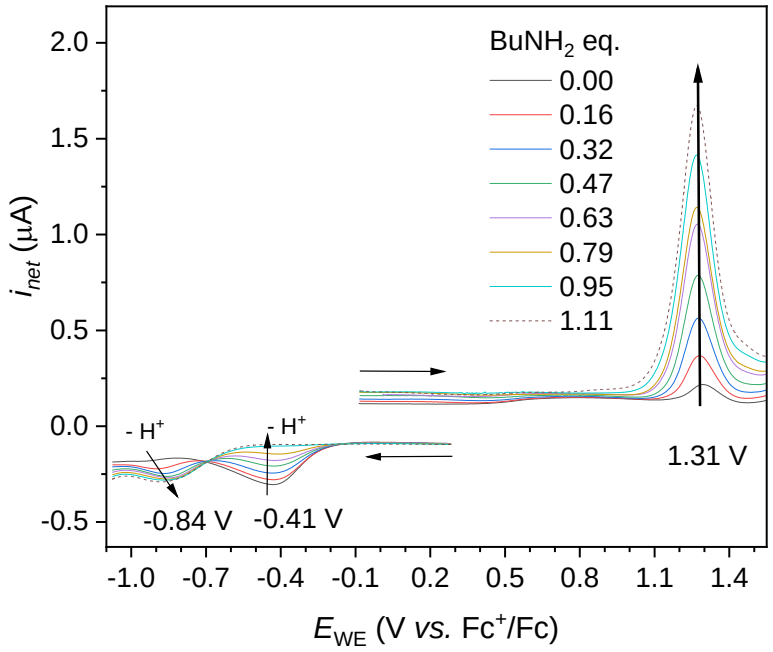

Figure S15. The cathodic and anodic branch of SWV upon addition of *n*-butylamine to **1** in acetonitrile (same conditions as in Figure S16).

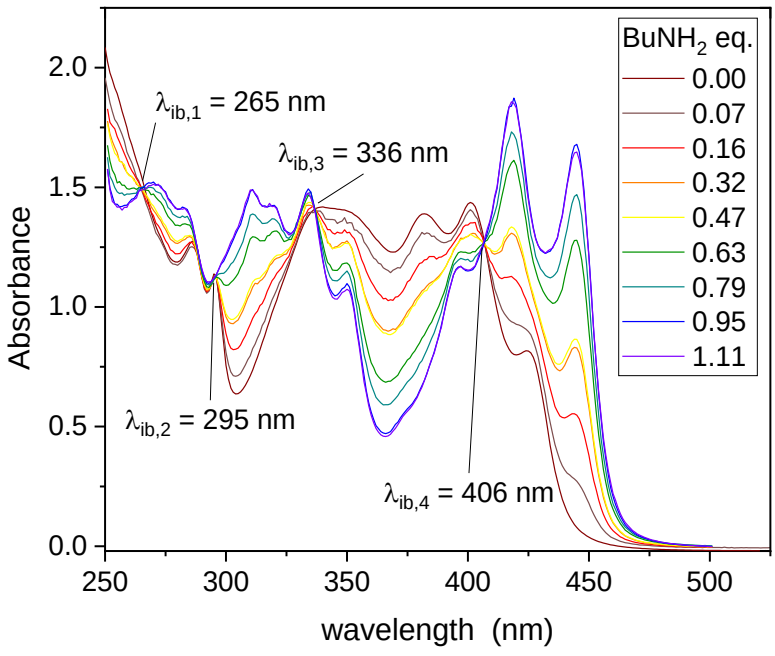

Figure S16. UV-visible absorption spectra measured during the titration of **1** (c = 0.075 mM) with *n*-butylamine in acetonitrile in the presence of 0.1 M TBAP.

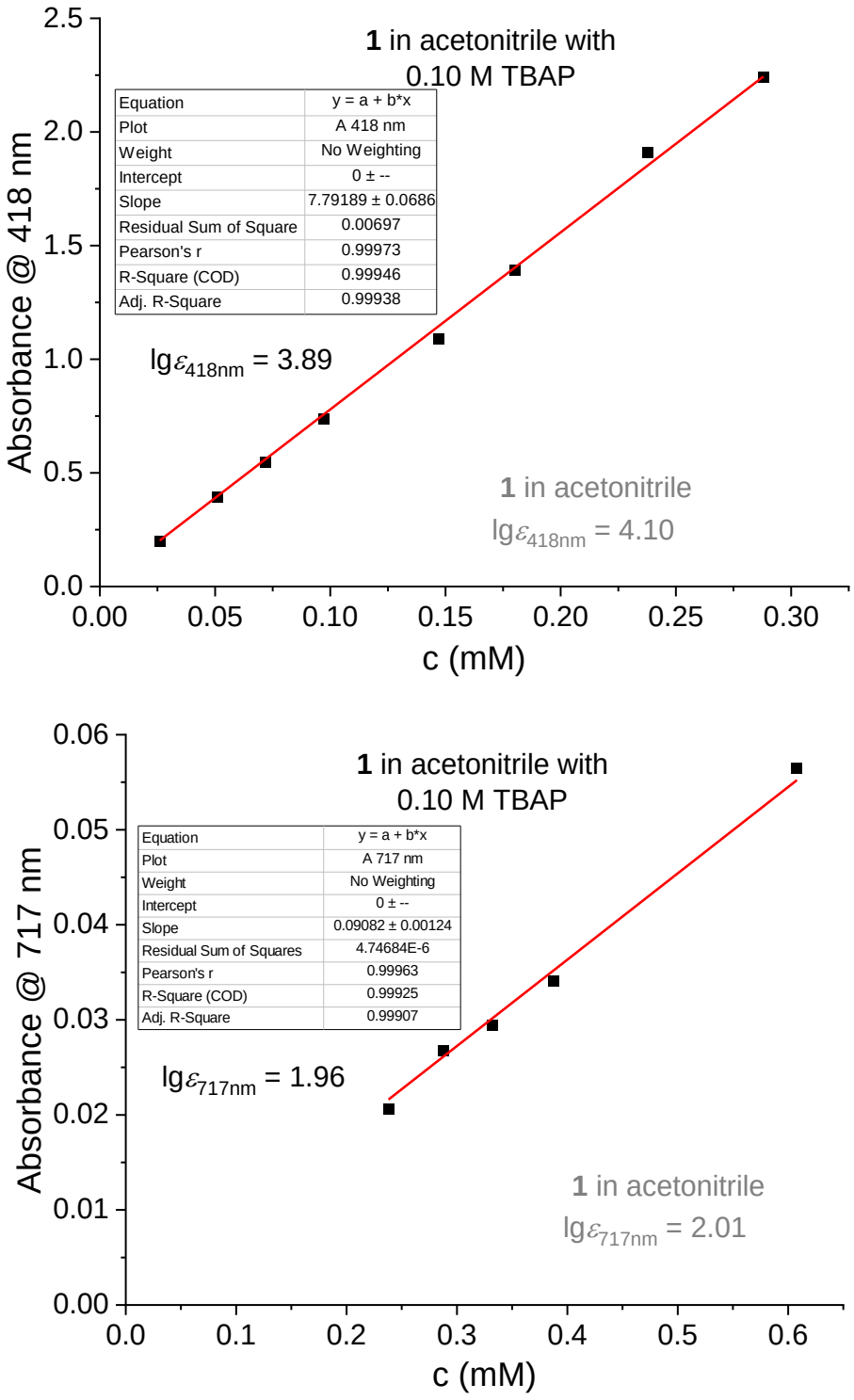

Figure S17. UV-vis absorbance of **1** at 418 nm and 717 nm in acetonitrile as a function of complex concentration in the presence of 0.1 M TBAP (lgε values in grey show the corresponding absorbance in the absence of TBAP salt).

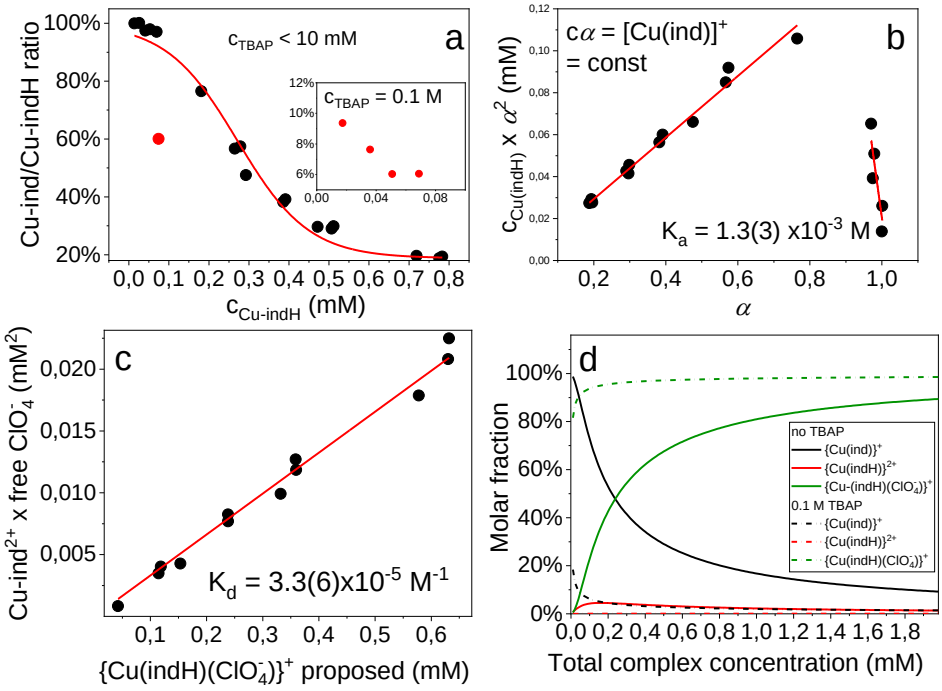

Figure S18. a) Deprotonation ratio according to the known molar absorptivity from the acid-base titration, demonstration of a buffering process; b) linearization of dissociation constant equation $c\alpha^2 = \kappa - \kappa\alpha$, demonstration that it only applies at large dissociation ratio and a linear part involving the protonated form c) correlation between the perchlorate coordinated form and free perchlorate indicating a dissociation equilibrium between $[Cu(indH)(OClO_3)]^+$ and $[Cu(indH)]^{2+}$; d) comparison of molar ratios without salt and in perchlorate containing solution.[2,3]

[2] Paixão, D. A.; de Oliveira, L. P.; da S. Maia, P. I.; Deflon, V. M.; Carneiro, Z. A.; de Almeida, K. J.; Lopes, N. P.; Pivatto, M.; Chaves, J. D. S.; de Albuquerque, S.; de Almeida, M. V.; Guilardi, S.; Guerra, W. Crystal Structure of Two New Polymeric Copper(II) Complexes Active against Trypanosoma Cruzi. *J. Saudi Chem. Soc.* **2018**, *22* (7), 809–815. https://doi.org/10.1016/j.jscs.2018.01.002.

[3] Rueda Espinosa, J.; Torres, J. F.; Gauthier, C. V.; Wojtas, L.; Verma, G.; Macías, M. A.; Hurtado, J. Copper(II) Complexes with Tridentate Bis(Pyrazolylmethyl)Pyridine Ligands: Synthesis, X-Ray Crystal Structures and ϵ-Caprolactone Polymerization. *ChemistrySelect* **2017**, *2* (30), 9815–9821. https://doi.org/10.1002/slct.201701820.

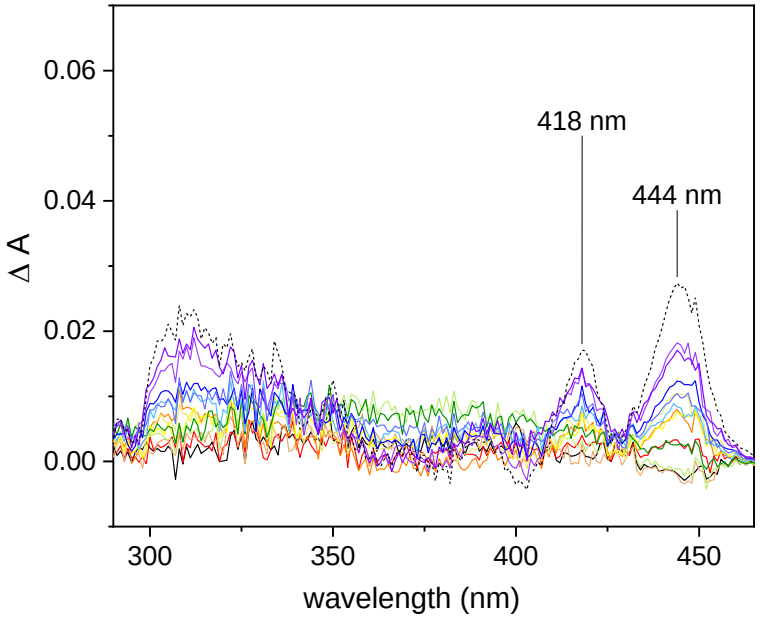

Figure S19. UV-visible difference spectra measured during bulk electrolysis at +1.52 V *vs*. Fc^+/Fc of **1** (c = 0.075 mM, 0.1 M TBAP) in acetonitrile, using a *l* = 1 cm immersion probe.

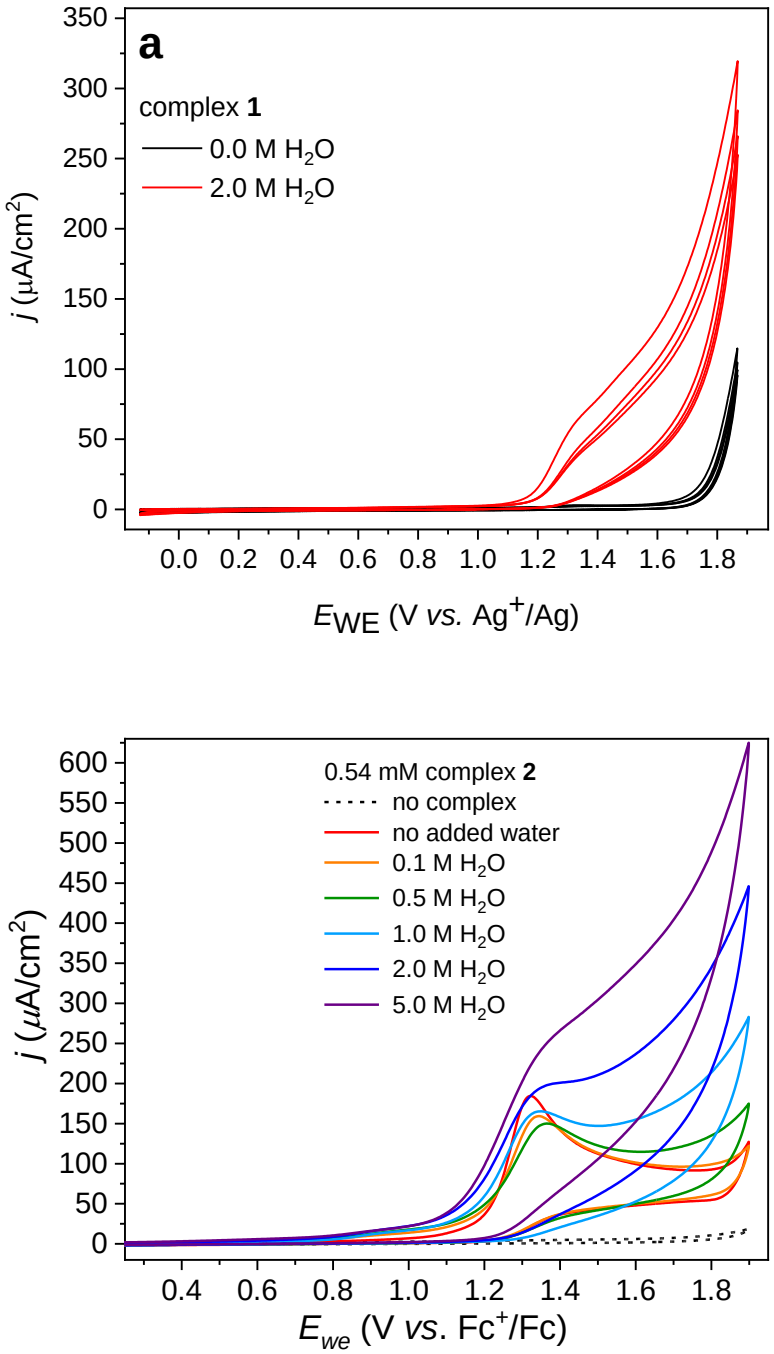

Figure S20. (a) CV of a 0.3 mM solution of **1** with no water and with 2.0 M of added water in acetonitrile, 0.1 M TBAP, BDD working and Pt aux. el., 100 mVs^{-1}; (b) CV of a 0.54 mM solution of **2** at different water concentrations in acetonitrile, this time using 0.1 M tetrabutylammonium hexafluorophosphate (TBAH) as salt, BDD working and Pt aux. el., 100 mVs^{-1}.

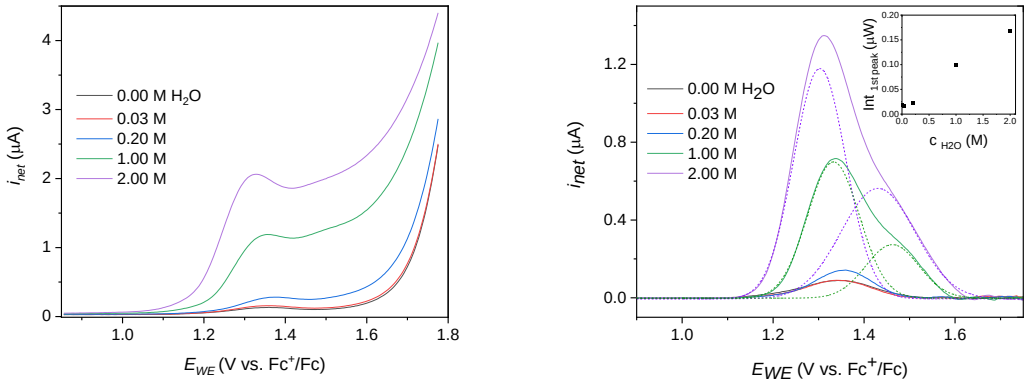

Figure S21. Dependence of SWV response on the concentration of water in the same solution as in Fig. S18 (on the left); baseline corrected SWVs, inset: variation of the i_{net} integral (μW) of the peak at lower potential with c_{H2O}.

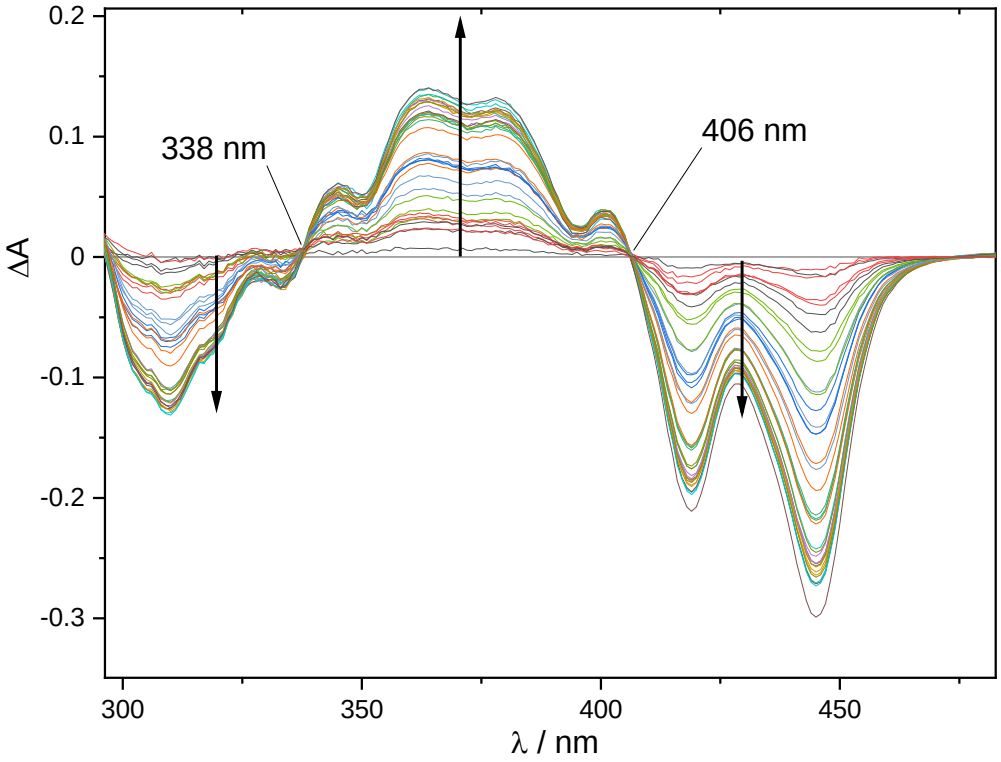

Figure S22. Changes in the UV-vis absorbance of a 0.063 mM solution of **1** in acetonitrile (0.1 M TBAP) containing 0.5(1) M water, upon sequenced CPE at +1.7 V *vs.* Ag^+/Ag org. ref. A sequence consisted of 3 minute CPE and 3 minute relaxation time at OCP. Three sequences are presented in the graph. The increase between 338 nm and 406 nm and decrease below 338 nm and above 406 nm is due to the accumulation of the protonated form. The reference spectrum is that of the stable system (after equilibration time).

Computational details of water oxidation in acetonitrile-water mixture

The free energy of every species was calculated as the sum of their single-point energy with the optimized structures and the thermochemical corrections derived from the frequency calculations at the temperature of 298.15 K and the pressure of 1 atm. Moreover, for molecules in the solution, a correction of –1.89 kcal/mol was employed to convert their concentration from 1 atm to 1 M. Specially, a –2.30 kcal/mol correction was used for H_2O because of its concentration of 2 M in the experiments. A detailed derivation of this correction could be found in the SI of this paper.[4]

To calculate the free energy changes of PCET steps, it is essential to acquire the standard free energy of proton and its concentration (i.e. pH) under catalytic conditions. The free energy of proton in gas phase is calculated as 6.3 kcal/mol based on Fermi-Dirac formalism[5] In aqueous solutions, the absolute solvation free energy of the proton is widely advocated to be –265.9 kcal/mol,[6,7] which could be directly employed in practical calculations. This value is derived from a lot of experimental data, and the accuracy could be satisfied. But in our case, the properties of proton in the acetonitrile-water mixture are rarely reported, and the DFT computations can hardly get the accurate energy of proton in such a nonstandard solution.[8] Therefore, here we choose to estimate these two values based on our computational and experimental results. We assumed that the acid-base dissociation constant of $[Cu^{II}(indH)(OClO_3)]^+$ discussed above would be maintained when the $(OClO_3)^-$ is replaced by H_2O, then the dissociation reaction could be written as

$$[Cu^{II}(indH)(H_2O)]^{2+} = [Cu^{II}(ind)(H_2O)]^+ + H^+$$

The standard free energy change of this reaction could be calculated based on its equilibrium constant $K = 8.5(4)\times10^{-7}$ (~5% std. error) as

$$\Delta G^0 = -RT\ln K = -8.314 \times 298.15 \times \ln(8.5\times10^{-7}) \times 10^{-3}\ \text{kJ/mol} = 34.63\ \text{kJ/mol}$$

Then the standard free energy of H^+ could be determined with the DFT calculated free energy of $[Cu^{II}(indH)(H_2O)]^{2+}$ and $[Cu^{II}(ind)(H_2O)]^+$ as

$$\Delta G^0(H^+) = 34.63\ \text{kJ/mol} + \Delta G^0([Cu^{II}(indH)(H_2O)]^{2+}) - \Delta G^0([Cu^{II}(ind)(H_2O)]^+)$$

[4] B. Rudshtein, K. J. Fisher, H. M. C. Lant, K. R. Yang, B. Q. Mercado, G. W. Brudvig, R. H. Crabtree, V. S. Batista, Water-Nucleophilic Attack Mechanism for the CuII(pyalk)2 Water-Oxidation Catalyst, *ACS Catal.* **2018**, 8, 9, 7952–7960. DOI: 10.1021/acscatal.8b02466

[5] J. J. Fifen, Z. Dhaouadi, M. Nsangou: Revision of the Thermodynamics of the Proton in Gas Phase, *J. Phys. Chem. A* **2014**, 118, 46, 11090-11097. DOI: 10.1021/jp508968z

[6] M. D. Tissandier, K. A. Cowen, W. Y. Feng, E. Gundlach, M. H. Cohen, A. D. Earhart, J. V. Coe, T. R. Tuttle, The Protons' Absolute Aqueous Enthalpy and Gibbs Free Energy of Solvation from Cluster-Ion Solvation Data, *J. Phys. Chem. A* **1998**, 102, 40, 7787-7794. DOI: 10.1021/jp982638r

[7] C. P. Kelly, C. J. Cramer, D. G. Truhlar, Aqueous Solvation Free Energies of Ions and Ion−Water Clusters Based on an Accurate Value for the Absolute Aqueous Solvation Free Energy of the Proton, *J. Phys. Chem. B* **2006**, 110, 32, 16066-16081. DOI: 10.1021/jp063552y

[8] Z. Marković, J. Tošović, D. Milenković, S. Marković, Revisiting the solvation enthalpies and free energies of the proton and electron in various solvents, *Comput. Theor. Chem.* **2016**, 1077, 11-17. https://doi.org/10.1016/j.comptc.2015.09.007.

Furthermore, the concentration of proton is also estimated with this equilibrium constant. In section 3.2 of the manuscript, the electrochemical tests were performed at 0.3 mM complex concentration with 2 M water present. Under this condition, the concentration of proton could be calculated as roughly 0.02 mM and the relevant pH is 4.66. This value is used to correct the potentials of PCET steps with the Nernst equation ($U = U^0 - 0.059 \times \mathrm{pH}$).

Table S4. Relative energy of the intermediates with alternative spin states.

Intermediate	Lower Energy Spin State	Higher Energy Spin State	Δ*G* (kcal/mol)
I1	doublet	quartet	47.0
I2	triplet	singlet	2.1
I3	quartet	doublet	3.5
I4	doublet	quartet	42.0
I5	triplet	singlet	21.3
I6	quartet	doublet	2.3

Specifically, the higher energy spin states of species **I3** and **I6** involve the antiferromagnetic coupling between the reactant and the Cu^{II}.

Table S5. $<S^2>$ values for intermediates with the lower energy state and the Becke spin population of the Cu center.

Intermediate	Ideal $<S^2>$	$<S^2>$	Cu spin population
I1	0.750	0.753	0.67
I2	2.000	2.049	0.68
I3	3.750	3.807	0.70
I4	0.750	0.754	0.59
I5	2.00	2.011	0.62
I6	3.750	3.762	0.70

The computational $<S^2>$ values are close to the ideal value, which indicates that all these intermediates are correctly converged to the target spin state. The spin population results show that the Cu center always has one unpaired electron during the reaction, which is corresponding to the Cu(II) ion.

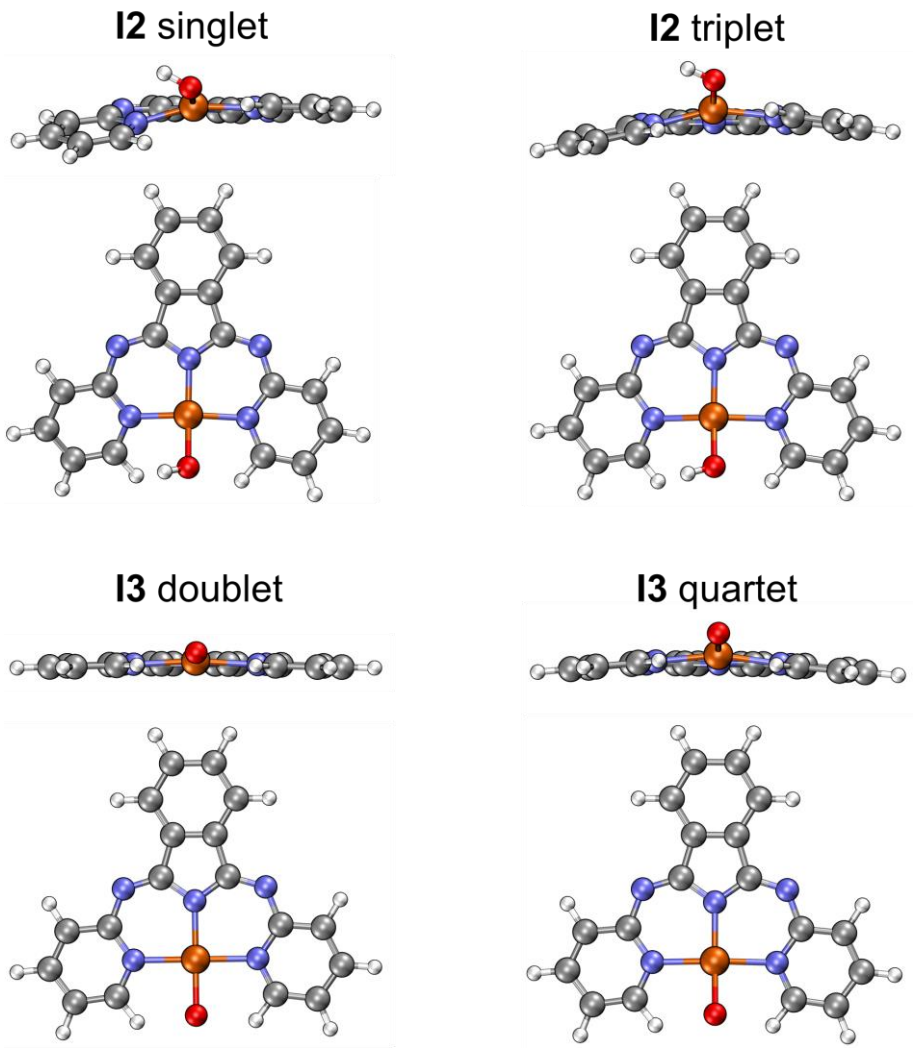

Figure S23. Front and top views of intermediates **I2** and **I3** with different spin states. Colour code: orange for Cu, red for O, blue for N, grey for C, and white for H.

Computational details of SET-WNA transition state

The energy barrier of SET-WNA process has been calculated to investigate the kinetics properties of water oxidation electrocatalyst. In intermediate **I3** ($[(L^{\bullet})Cu^{II}(O^{\bullet -})]^{+}$), the oxyl radical would be nucleophilically attacked by an adjacent water molecule, then the oxyl radical would provide an electron to reduce in ligand and form O–O bond with the oxygen in the water molecule as the Type 3 SET-WNA mechanism shown in our manuscript.

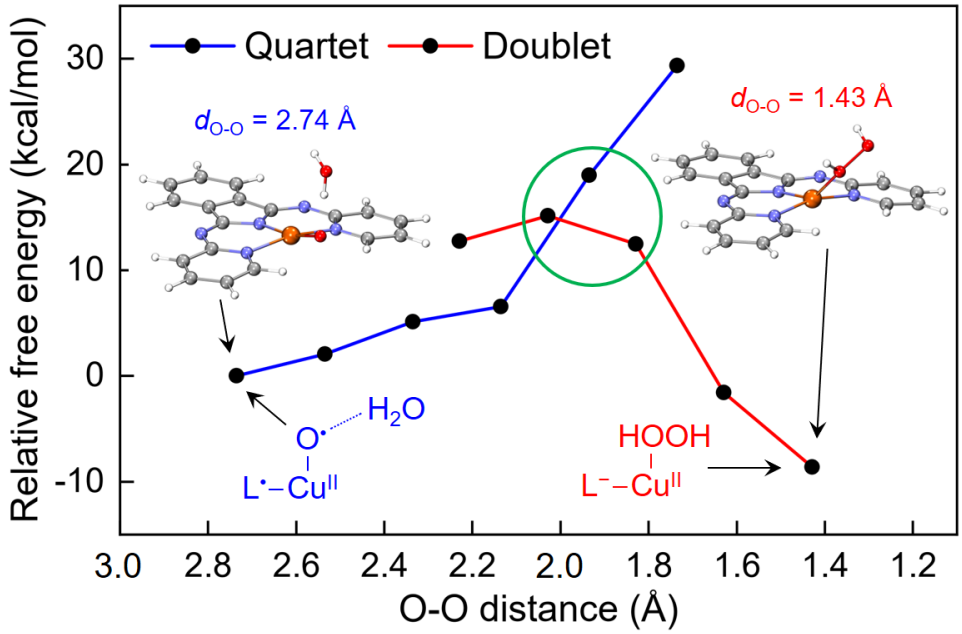

Figure S24. Free energy relaxed scan for O–O bond formation. The green circle indicates the cross between the quartet and doublet states at a O–O distance of about 2.0 Å.

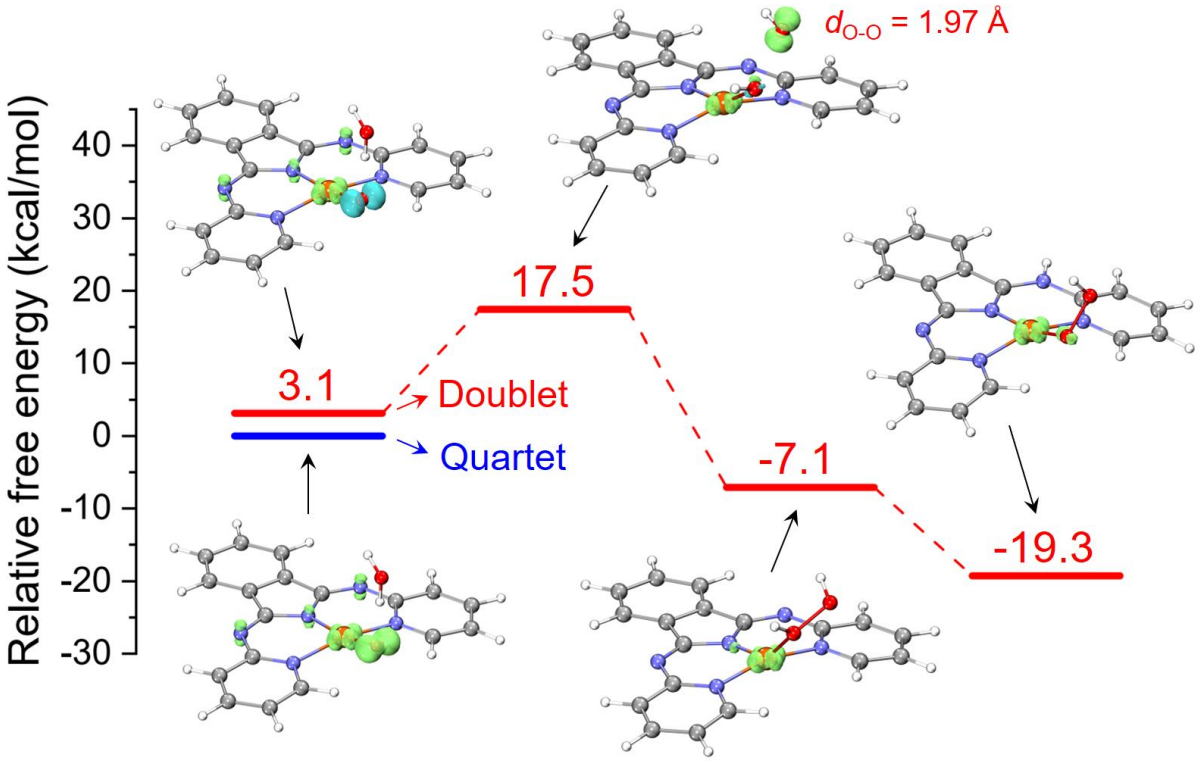

Figure S25. Free energy diagram of SET-WNA process and the structures of each intermediate. The green and blue regions indicate the iso-surface of spin charge density with spin up and down charges (iso-value 0.05).

Coordinates of Structurally Optimized Molecules

The following list contains the .xyz coordinate files of the intermediates in catalytic cycle

39
I1 $[Cu^{II}(ind)(OH_2)]^+$

C	6.07805790567671	-0.09785595432614	4.31143155562331
C	6.68674997259722	-1.10709034565370	5.20496224602351
C	7.40976623618428	-2.26436324603976	4.93665013916412
H	7.61712768047699	-2.57500013733012	3.91034358735033
C	7.85835945626688	-3.01395949962074	6.03351205574717
H	8.42722838011648	-3.93111399444520	5.86234050994394
C	7.58893494253354	-2.60693913374490	7.35022783787605
H	7.95343450455510	-3.21365839439925	8.18273605193590
C	6.86254487649559	-1.43657005712110	7.61296133928061
H	6.65203900429664	-1.11277477975727	8.63454721632972
C	6.41766925322312	-0.70044020027138	6.52018869101205
C	5.64813346230912	0.55925673620809	6.43036376884491
C	5.60519387819687	0.78690785110582	2.16844579953492
C	5.91281075021405	0.63420213269977	0.79656086763614
H	6.52593760153112	-0.22139711416198	0.51188319992579
C	5.45281366553839	1.54986126295477	-0.13504593812331
H	5.69559815971701	1.42950918653002	-1.19340260107318
C	4.67629094131169	2.63266175461949	0.30099854160501
H	4.29657225484798	3.38656398190322	-0.38977451340406
C	4.38998618771014	2.73073282217181	1.65299476625334
H	3.78971056621990	3.56057482994550	2.03284095560494
C	4.56037790954486	2.42131393331269	7.40154136051457
C	4.36623391552492	3.09297644127732	8.63061045996434
H	4.74570993443472	2.61047033844152	9.53179147350878
C	3.73052273721210	4.32272353672738	8.66863416361227
H	3.59013733241723	4.84173564566872	9.61964968963419
C	3.27570855261955	4.89135632011203	7.47077813402721
H	2.77722008668074	5.86104011497610	7.44459065360764
C	3.47163259362144	4.18534638221447	6.29502333297999
H	3.13030645006424	4.59368075287885	5.34096582223062
N	5.48533345049610	0.85576355856380	5.10037267991348
N	6.13306988736637	-0.15168493864561	3.01843710765458
N	4.82669200034262	1.83318270914275	2.56304093515308
N	5.23748921659697	1.22955873329291	7.45981081809346
N	4.08495450557230	2.98240031806848	6.25446147614884
Cu	4.28124175863032	2.16740998411213	4.44928977158805
O	2.34007330383804	2.68592380658463	3.89261800997939
H	1.94530908609756	2.24976841002439	3.11514114440301
H	1.64602759892073	2.69792625198038	4.57747688989498

38
I2 $[Cu^{II}(ind)(OH)]^+$

C	6.07938766488209	-0.05636162023064	4.32429263299550
C	6.68879879077742	-1.07018080763915	5.19886841150666

C	7.45216310199149	-2.20083575836794	4.92651535959341
H	7.70449836976767	-2.48145268006190	3.90197540509815
C	7.88132447669793	-2.96251085200024	6.02192299686531
H	8.48048024236367	-3.85987481704900	5.85057651703473
C	7.55591734992706	-2.59406996875037	7.33810949326057
H	7.90774648268164	-3.21172252523017	8.16771601303054
C	6.79140932655157	-1.44993807680135	7.60535071435088
H	6.53978732783081	-1.15710098347381	8.62663381833677
C	6.36432281774097	-0.70175761403719	6.51346969994415
C	5.57916934432973	0.53851868166196	6.41260859371652
C	5.63472718731295	0.80261896685456	2.14505288082252
C	6.02621843127407	0.65400746058253	0.79083299666995
H	6.73666409317814	-0.13807477357555	0.55257978908291
C	5.51010541099188	1.50374617940032	-0.18115611465935
H	5.81082325453208	1.40097776452351	-1.22566211007663
C	4.59465396180419	2.47848474684770	0.21048557606547
H	4.14713023461479	3.16727029186792	-0.50764118147866
C	4.23361338280487	2.56859187205802	1.56519071958327
H	3.49746056487331	3.29792859988748	1.90990285094280
C	4.50006396568173	2.40191216301140	7.43134472509264
C	4.34127933341067	3.03183867386569	8.68808506798815
H	4.69783539037565	2.49928262540428	9.56994081471272
C	3.77402932447240	4.29873383128118	8.76679199395272
H	3.66047883446365	4.79703045948760	9.73164393164508
C	3.36034985274620	4.91548409859157	7.58738621112496
H	2.91606730055000	5.91169838799847	7.58394713987924
C	3.50906785465443	4.22618809449040	6.37635891975715
H	3.17367187984651	4.67535685091127	5.43976583587703
N	5.42841268019496	0.86960592857663	5.08869599158613
N	6.19812033730379	-0.07055404730019	3.01917113298754
N	4.73677437835100	1.76750806109799	2.50288453593404
N	5.15097791237551	1.20509332068607	7.45013297632561
N	4.04813324764382	3.00690367074011	6.29481041845588
Cu	4.11085019532576	2.14356752397439	4.43611323337652
O	2.50035803761603	2.87772269763219	3.80800373500769
H	1.87212765805945	3.08536357308421	4.51429827361131

37

I3 $[Cu^{II}(ind)(O)]^{+}$

C	6.13490042506724	-0.04286683263137	4.32199610023518
C	6.74277497837565	-1.05533974306808	5.19910789493488
C	7.44271580154009	-2.22653163137608	4.92847671549975
H	7.63634795140927	-2.54808941725902	3.90316879567971
C	7.88657040194416	-2.97507994076519	6.02715309806610
H	8.44017462458122	-3.90154258735490	5.85761068889646
C	7.63135969123552	-2.55831549577569	7.34450305849280
H	7.99220825155216	-3.16769868745253	8.17635006165268
C	6.92337982999384	-1.37801176708579	7.60968961910657
H	6.72135849886756	-1.05071077096179	8.63153277657300
C	6.48779482827023	-0.63901876231422	6.51470699901096
C	5.73113179151917	0.61816939932648	6.40952103400029

C	5.62344848355650	0.76651318580487	2.13500799941058
C	5.69916266598937	0.38877304333594	0.77208182085861
H	6.18766093314123	-0.55693429374945	0.53664772724624
C	5.15387685294485	1.20519360402159	-0.21220753759408
H	5.20501809323976	0.91733362483612	-1.26417783094328
C	4.54502764876264	2.39599662574347	0.17829553443394
H	4.10027859481921	3.08000924707883	-0.54587767898239
C	4.50779949681923	2.72237697310279	1.54198863814417
H	4.03772669850062	3.65070030924397	1.87690854658157
C	4.58799995646317	2.44131638987990	7.44375745675984
C	4.17085182981806	2.90515057624613	8.71531295362437
H	4.47570301143045	2.32744552248380	9.58811171252271
C	3.39178253592482	4.05182351045134	8.82141314842387
H	3.06454211112358	4.41296865027990	9.79835766681246
C	3.04121376803096	4.72385042714174	7.65242943192355
H	2.43044778743040	5.62766420614469	7.66880187376851
C	3.49491834131264	4.22540904709540	6.42223941583493
H	3.24153875923602	4.73621117124332	5.48986151149541
N	5.54926783357269	0.92771626926197	5.08885045225708
N	6.16283790597162	-0.11668498847292	3.01638045167433
N	5.03026469444198	1.94441326934487	2.49244612632518
N	5.30940647947596	1.28914086146745	7.45044075382508
N	4.24946206366788	3.12987483916415	6.31326076528898
Cu	4.87370719792538	2.62613120684000	4.42314018237158
O	4.65033918204431	4.38564295872822	3.84071203578786

40

I3 initial state in TS calculation $[Cu^{II}(ind)(O)(H_2O)]^+$

C	6.18002549105760	-0.11843652256789	4.35102760487905
C	6.72043249144003	-1.17106816913845	5.22285612244360
C	7.37522862569950	-2.36708086658512	4.94701735442348
C	7.75708370331531	-3.15352672885297	6.04215220530191
C	7.48631311077801	-2.74966862610819	7.36081568067955
C	6.82405989306048	-1.54467046389178	7.63121772941486
C	6.45004324708012	-0.76779459402751	6.53957256966963
C	5.75496915111428	0.52319591808021	6.44042185977393
C	5.74542897193709	0.73631585196581	2.16709400717126
C	5.84037906839421	0.38201042446573	0.79902975866525
C	5.33493934959600	1.23042848875397	-0.18026888407052
C	4.74740366333863	2.42792173060020	0.22037358101016
C	4.69472927730398	2.73217748739169	1.58962336842716
C	4.68674047679334	2.38103804230484	7.48862863934509
C	4.27308708679703	2.84953809466583	8.75977736995177
C	3.57300486272123	4.04605407445357	8.87101202599682
C	3.29785310082796	4.76183125636668	7.70847813777528
C	3.74123828412392	4.25252099106860	6.47793880374232
H	7.58134906112525	-2.67823766460773	3.92098123423494
H	8.27423080800294	-4.10012864276751	5.86921285837585
H	7.79874493852254	-3.38947748155664	8.18934003066297
H	6.61028881845203	-1.22697132836067	8.65364570898883
H	6.30856624874051	-0.57191050630153	0.55558548861532

H	5.39938525257747	0.96045602540559	-1.23621379134690
H	4.33200376849132	3.13521104119430	-0.49875465600896
H	4.24491800954138	3.66804601944851	1.93266857620923
H	4.51892425050840	2.23746836361874	9.62776256045785
H	3.24907415212490	4.41166942257241	9.84733747877149
H	2.75260378721065	5.70633919595047	7.72853177991248
H	3.54306721179814	4.79560257869940	5.54967475488931
H	7.75282389962184	5.31053991176621	4.23248974335000
H	6.25206420564465	5.31772806481159	3.84035185378772
N	5.62106106749017	0.86533761882210	5.12193353993551
N	6.23671822979855	-0.17585156810821	3.04486593296075
N	5.17773429655086	1.92333881737049	2.53404741718005
N	5.34041043845299	1.19105359348677	7.48704480895251
N	4.41590941495456	3.10777145423358	6.36413207292107
Cu	5.00183549120588	2.58471867766555	4.46830373710569
O	4.78808488045000	4.36748440226656	3.87748835350843
O	7.07824191335571	5.86102561544469	3.80780258193476

40

I3 TS [Cu^{II}(ind)(HO)(OH)]$^{+}$

C	0.69247237209694	-1.53262564049372	-0.60244405293783
C	1.18757432107178	-2.60349679060901	0.28195803884925
C	1.80180283237558	-3.82080489513336	0.00773223222507
C	2.17074721537815	-4.61390661990754	1.10351891241874
C	1.91568601231859	-4.19982425248327	2.42152738149805
C	1.28122085565413	-2.97853017624356	2.68902433212390
C	0.93118266909028	-2.19165929099362	1.59689364632205
C	0.28411382171524	-0.87018469556516	1.50976491017436
C	0.17432529965511	-0.67701580638553	-2.74447194987227
C	0.22693338788282	-1.00954186952550	-4.11823493666176
C	-0.30800516671914	-0.16129589391958	-5.07185970886756
C	-0.90849200048594	1.02969688750304	-4.64602183106197
C	-0.93218994428646	1.31892288092770	-3.28842612829509
C	-0.81401579836957	0.97483933667552	2.48810246084622
C	-1.27096746070135	1.47611835870799	3.72943348760608
C	-1.97405521327785	2.66810237514399	3.79010513398729
C	-2.21145528388214	3.36592535166547	2.60186244916338
C	-1.72804903738509	2.84215742713015	1.40523202119599
H	1.99399984920954	-4.14029096410712	-1.01863740227528
H	2.66866632932456	-5.57118098941227	0.93078683015090
H	2.22091728859100	-4.84144249793198	3.25172232173106
H	1.07672343624740	-2.65259924527346	3.71105280453451
H	0.70772456810578	-1.95240106840329	-4.38179346007367
H	-0.26776599101553	-0.42209438433085	-6.13196821682223
H	-1.36893789762681	1.72536812797280	-5.34944823120862
H	-1.41548899296881	2.22968741970797	-2.93143472131618
H	-1.03577874093352	0.89106074932047	4.61923173002909
H	-2.33375346114304	3.05079334680935	4.74772496140350
H	-2.77834801070400	4.29813166381100	2.58741766679232
H	-1.89399012396237	3.36017298403995	0.46093034800726
H	1.72035582199661	3.58954144469792	0.10081750037402

H	0.20348425829010	3.11985826585249	-1.85037563045647
N	0.22264023180618	-0.50994234136478	0.18630272182647
N	0.70768028712676	-1.60159435524994	-1.89481634521028
N	-0.40118279457905	0.50019010632254	-2.35355284091051
N	-0.14660847527049	-0.21292662194026	2.53937868376611
N	-1.05489587798756	1.67841208343138	1.34365694053224
Cu	-0.38674259483023	1.15321182797093	-0.47005722179498
O	-0.13900356541877	2.99094435315727	-0.94798378503503
O	1.18147557361116	4.30022340842588	-0.30265105275811

40

I3 final state in TS calculation [Cu^{II}(ind)(HOOH)]$^{+}$

C	5.66670040650892	0.57859808974425	6.44222045847705
C	6.41486207888086	-0.69460903638110	6.52825162853255
C	6.85901764418336	-1.43421083349629	7.61895386414834
C	7.56214380023791	-2.61803185137103	7.35290778687450
C	7.80857879803497	-3.03568202017821	6.03517565986486
C	7.36031215409691	-2.28317390624924	4.93998902328313
C	6.66157190926674	-1.11187285844600	5.21116989258000
C	6.06454773990458	-0.09400896253193	4.31918837538293
C	4.61215671476263	2.46201962805152	7.41234122128940
C	4.38981951583904	3.11610505073987	8.64636506754856
C	3.76393020724376	4.35059522203856	8.68798850095000
C	3.35222680950531	4.94776536486137	7.48811480766989
C	3.58061592769630	4.26403214607610	6.30570538756512
C	5.59056319169535	0.80722794737341	2.18374738728176
C	5.86613454767381	0.64512312060629	0.80675032263938
C	5.42031466245009	1.57792858424469	-0.11512888733357
C	4.68905451179146	2.68644404656696	0.33377724164529
C	4.42791644958634	2.79232213964010	1.68987781432744
H	6.66682825965324	-1.10288366486423	8.64165191055992
H	7.92655933170465	-3.22662857642891	8.18417652363855
H	8.36009597678910	-3.96303344075009	5.86182762778306
H	7.55100964037691	-2.60183593221622	3.91300547616623
H	4.73805828951014	2.61416493552746	9.54951539932592
H	3.59845800173297	4.85276573964848	9.64395541755083
H	2.86509042737108	5.92339651103315	7.46549034722223
H	3.28149943394624	4.69942483336585	5.34867215524687
H	6.44539129670520	-0.22974134730356	0.51025582903275
H	5.64011914512847	1.45079328838102	-1.17769180363101
H	4.32382060431603	3.45333800255396	-0.35044372553937
H	3.85471697352519	3.63558355101236	2.08098186056093
H	1.76618389863773	1.23658368426584	2.97554671663897
H	1.65066688665262	2.83988385533521	4.70082019021515
N	5.49859775959402	0.87084638400269	5.11317376683399
N	5.27144615232964	1.26070915808865	7.47013993634358
N	4.17902316171658	3.05253716223800	6.26186648615406
N	6.10521471720511	-0.14605486404717	3.02585852066006
N	4.85314802550293	1.87967931310162	2.59031316632135
Cu	4.37866633577259	2.25118156237721	4.46708984438249
O	2.33348720029915	2.73377725552614	4.00488301236545

O	1.62245141217101	2.20194071786304	2.88551578944029

40

I4 [Cu^{II}(indH)(OOH)]$^{+}$

C	6.03504598708377	-0.10033355787806	4.35729961466803
C	6.66000863755743	-1.12014706482837	5.21119027336494
C	7.38458728482309	-2.27644679167727	4.93866671180562
H	7.59505651987216	-2.60709729693163	3.91874619038096
C	7.84223775069391	-3.01899365425989	6.03660895449371
H	8.41145707023642	-3.93491945433387	5.86370379989989
C	7.58122347319702	-2.60572098749487	7.35165611085502
H	7.95341079158493	-3.20746584382150	8.18404910910142
C	6.85389062131110	-1.43534992245409	7.61624534027471
H	6.65174587464300	-1.10762670073429	8.63795419390394
C	6.39747596599700	-0.70598625760401	6.52654825203208
C	5.62944483676065	0.55277127963067	6.43388568427086
C	5.60898193653416	0.80536981930376	2.09353854897700
C	5.98022933334679	0.61017025164943	0.75423922750674
H	6.59989979863802	-0.24668885689832	0.48394272972800
C	5.55223945348592	1.52696806431005	-0.19570195854645
H	5.83073010115871	1.39905823527389	-1.24388660290161
C	4.76825509833561	2.61152691611250	0.21226096555041
H	4.41413536431560	3.36014219303659	-0.49762709758649
C	4.43423852396426	2.72098472656050	1.55484520053747
H	3.80657385526951	3.53261035636385	1.92425241936347
C	4.57755175695215	2.44605803247363	7.41833021491427
C	4.46328093779272	3.11165707186829	8.65475718451679
H	4.89489777088558	2.63156179562380	9.53336059293848
C	3.82603018690568	4.34383752490154	8.72633914540627
H	3.74242441998405	4.86838591597344	9.68086368720541
C	3.29139185960320	4.89274347605028	7.55815245750447
H	2.77821108896205	5.85541569759916	7.55745088927704
C	3.41469376591686	4.17605931630322	6.37183723726727
H	2.98175504939711	4.55161441423502	5.44256894139863
N	5.44029006127411	0.84249278020411	5.07897282731659
N	6.08355522416641	-0.12326196976006	3.02492890208383
N	4.84063216266305	1.83289176314684	2.48428580204406
N	5.25252723173099	1.24144226427469	7.44753589316830
N	4.04214209350480	2.99051820952908	6.29615641228298
Cu	4.15908336907308	2.16641917729614	4.41938273691498
O	2.57254355454202	3.09341286995454	3.86851307927281
O	1.85275757351412	2.20468140996567	2.99432993787914
H	1.18380542760650	1.82235085301884	3.59085868633805
H	6.58904818671624	-0.90559605598336	2.61419770459073

39

I5 [Cu^{II}(indH)(OO)]$^{+}$

C	6.13680802198309	-0.00461303967116	4.30990976989938
C	6.79853362343970	-0.98718125377544	5.19494850481746
C	7.54709579822230	-2.12442910102985	4.92456598010480
H	7.74584484146958	-2.43735864168401	3.89752797902165

C	8.03681376354687	-2.85261912080853	6.01977074164607
H	8.63177523965193	-3.75183811777367	5.84370307825187
C	7.77580424890024	-2.44920681937553	7.33751515691332
H	8.17132748230717	-3.03779649654208	8.16811450439580
C	7.01549983751909	-1.30192157124171	7.60752339650350
H	6.81784524206075	-0.99698698092117	8.63800466124330
C	6.53699289210912	-0.58447772376429	6.51598276607178
C	5.72662987942874	0.63563945121545	6.38984100733679
C	5.50807216441982	0.80687103283653	2.15597414705734
C	5.50330439312803	0.40853598988710	0.80424792986092
H	5.99101366955716	-0.53293030121745	0.55036992694780
C	4.88701014232320	1.19956993643296	-0.15687165676039
H	4.87740499823547	0.89006686309516	-1.20444405661192
C	4.28746986262652	2.39654347870138	0.24218680772127
H	3.79150741938429	3.05813498086038	-0.46961848648054
C	4.33721007801035	2.74454562528972	1.58821159433314
H	3.89145992358996	3.67995343331467	1.93234093376631
C	4.42953897846902	2.46328875323878	7.45505843536761
C	3.95852499400454	2.86965894494450	8.71372649711651
H	4.25255503796202	2.31348127042762	9.60554548348483
C	3.11773600788063	3.97064366742907	8.79060585767822
H	2.73799375189819	4.30209352862050	9.75926744764116
C	2.76469329130689	4.64004842311140	7.61389026778665
H	2.10157513524970	5.50612232406232	7.62327412476890
C	3.28516425216484	4.18207480404667	6.41256361642143
H	3.04596585821962	4.68465948807891	5.47418098488315
N	5.51920231387880	0.94900529130302	5.11926947449593
N	6.13466978521664	-0.06281127838468	3.02861608921677
N	4.92480639545575	1.97917750084171	2.52429774670247
N	5.25417178098779	1.33302906475922	7.42563000869802
N	4.10943505207482	3.11727432147925	6.32597799650375
Cu	4.82432632349110	2.64349593691112	4.45003461538657
O	4.91418126159803	4.55842592798125	3.90960375256668
O	6.11291675277886	4.88337863462276	4.22749127520853
H	5.48411950544864	0.96445177269789	8.34616164003248

38

I6 [Cu^{II}(ind)(OO)]$^{+}$

C	6.15280276308283	-0.05645986644722	4.30276346227009
C	6.71101436950673	-1.08984670690587	5.20129258090954
C	7.39176223349582	-2.27269105383343	4.93539137918112
H	7.60123159769129	-2.58555157717970	3.91031846988301
C	7.79704990700500	-3.04468837148009	6.03363843242446
H	8.33476266745007	-3.98050742830867	5.86377172968277
C	7.52385939925316	-2.63721062112183	7.34905321672629
H	7.85407696684245	-3.26226725397350	8.18213400599051
C	6.83637565576970	-1.44338586044818	7.61097495947161
H	6.62189288438243	-1.12083301107778	8.63199421363686
C	6.43771979594199	-0.68182874951062	6.51818112970600
C	5.71545442808910	0.60554012886957	6.43227529591745
C	5.70197994535899	0.87969279633497	2.17638544202202

C	5.80602443552257	0.63836458400649	0.78830737963330
H	6.27771498519269	-0.29316211038609	0.47464931460861
C	5.31982592857695	1.55897621950622	-0.12578680713520
H	5.40168244854634	1.36454593612661	-1.19768900699324
C	4.72594415712755	2.74136434535843	0.33878379841624
H	4.33297694220113	3.49702430503489	-0.34232485195042
C	4.64862744605267	2.93967548417118	1.70677549380116
H	4.20067162719285	3.84934841949706	2.11708818935350
C	4.66096447315162	2.50585134510172	7.36870487507150
C	4.25110284408724	3.08675940749450	8.58953904792456
H	4.46749893223301	2.53608499723672	9.50529556303732
C	3.60173208610849	4.31048226044784	8.60486740903118
H	3.28883301808691	4.75444363719503	9.55261017119209
C	3.35443066404359	4.97293227998599	7.39391246875145
H	2.85108836799505	5.93955077421456	7.35667780473308
C	3.77200561567589	4.36741051498392	6.22103389363576
H	3.60520445813444	4.84691321866977	5.25203098836072
N	5.57184402903850	0.89817234953939	5.09929435187712
N	6.21008079421468	-0.08490037230389	3.01002924760637
N	5.11748177202776	2.03928127290236	2.59919102049258
N	5.30687790533860	1.29759679942263	7.44684280135349
N	4.40251288614152	3.17188192560127	6.20505188828224
Cu	4.85143512763102	2.50709938572664	4.45125204557674
O	2.35930061072800	0.93118683716732	4.41887307479180
O	2.16415583108049	-0.20884624161835	4.74181552072558

Table S6. Summary of the catalytic data of relevant complexes for water oxidation described in the literature

Catalyst	Mechanism	pH	Electrolyte	TOF_{max} (s^{-1})	η (mV)	Farad. eff. (%)	Ref.
$[(TAML)Cu]^{2-}$	SET-WNA	7	phosphate	140	200	n.a.	[37]
$[(L1)Cu]^{2-}$	SET-WNA Type 1	11.5	phosphate	3.56	700	47	[34]
$[(L2)Cu]^{2-}$	SET-WNA Type 1	11.5	phosphate	3.58	400	n.a.	[34]
$[(L3)Cu]^{2-}$	SET-WNA Type 1	11.5	phosphate	0.43	270	n.a.	[34]
$[(L4)Cu]^{2-}$	SET-WNA Type 1	11.5	phosphate	0.16	170	~100	[34]
$[(bpy)Cu(OH)_2]$	SET-WNA Type 2	12.8	NaOH/NaOAc	100	740	90	[36]
$[Cu(GGGG)(OH_2)]^{2-}$		11	phosphate	33	~650	99	[31]
$[(6,6'\text{-dhbpy})Cu(OH_2)_2]$	SET-WNA Type 1	12.4	NaOH/NaOAc	0.4	640	85	[35]
$[Cu(Lpy)(OCO_2H)^-]$	WNA	10	carbonate	20.1	650	95	[55]
$[Cu(pyalk)_2]$	SET-WNA	12.5	KOH	0.7	520 - 580	75	[9]
Cu-porphyrin	SET-WNA	7	phosphate	30	310	93	[10]
[**2**]	SET-WNA Type 3	10	carbonate	6.95*	970	69	This work

Ligands abbreviation used: TAML (tetra-amidate macrocyclic ligand) = 15,15-dimethyl-8,13-dihydro-5*H*-dibenzo[*b*,*h*][1,4,7,10]tetraazacyclotridecine-6,7,14,16(15*H*,17*H*)-tetraone; L1–L4 = N1,N10-(4,5-R-1,2-phenylene)*bis*(N2-methyloxalamide), R1,R2 = H for L1; R1,R2 = CH_3 for L2; R1 = OCH_3, R2 = H for L3 and R1,R2 = OCH_3 for L4; bpy = 2,2′-bpy; GGGG = triglycylglycine; 6,6′-dhbpy = 6,6′-dihydroxy-2,2′-bpy; L_{py} = 4-pyrenyl-1,2-phenylenebis(oxamidate); pyalk = 2-pyridyl-2-propanoate; porphyrin = tetrakis(4-N-methylpyridyl)porphyrin.

*a value of 6.95 h^{-1} could be determined from product detection upon CPE

[9] Fisher, K. J.; Materna, K. L.; Mercado, B. Q.; Crabtree, R. H.; Brudvig, G. W. Electrocatalytic Water Oxidation by a Copper(II) Complex of an Oxidation-Resistant Ligand. *ACS Catalysis* **2017**, 7 (5), 3384–3387. https://doi.org/10.1021/acscatal.7b00494.

[10] Liu, Y.; Han, Y.; Zhang, Z.; Zhang, W.; Lai, W.; Wang, Y.; Cao, R. Low Overpotential Water Oxidation at Neutral PH Catalyzed by a Copper(II) Porphyrin. *Chem. Sci.* **2019**, 10 (9), 2613–2622. https://doi.org/10.1039/C8SC04529A.